Following the flare of PKS 1502+106 with mm-VLBI imaging and light curve modelling

Vassilis Karamanavis

Max Planck Institute for Radio Astronomy

With: L. Fuhrmann, T. P. Krichbaum, E. Angelakis, I. Myserlis, J. Hodgson, B. Boccardi, I. Nestoras, J. A. Zensus, H. Ungerechts, and A. Sievers

13th European VLBI Network Symposium and Users Meeting | September 23, 2016 | St. Petersburg, Russia

Why PKS 1502+106?

- FSRQ with $M_\bullet \approx 10^9\ M_\odot$ at z = 1.839

- Motivation:

  In 2008 *Fermi*/LAT discovered a bright high-energy flare from PKS 1502+106

- followed by delayed radio emission

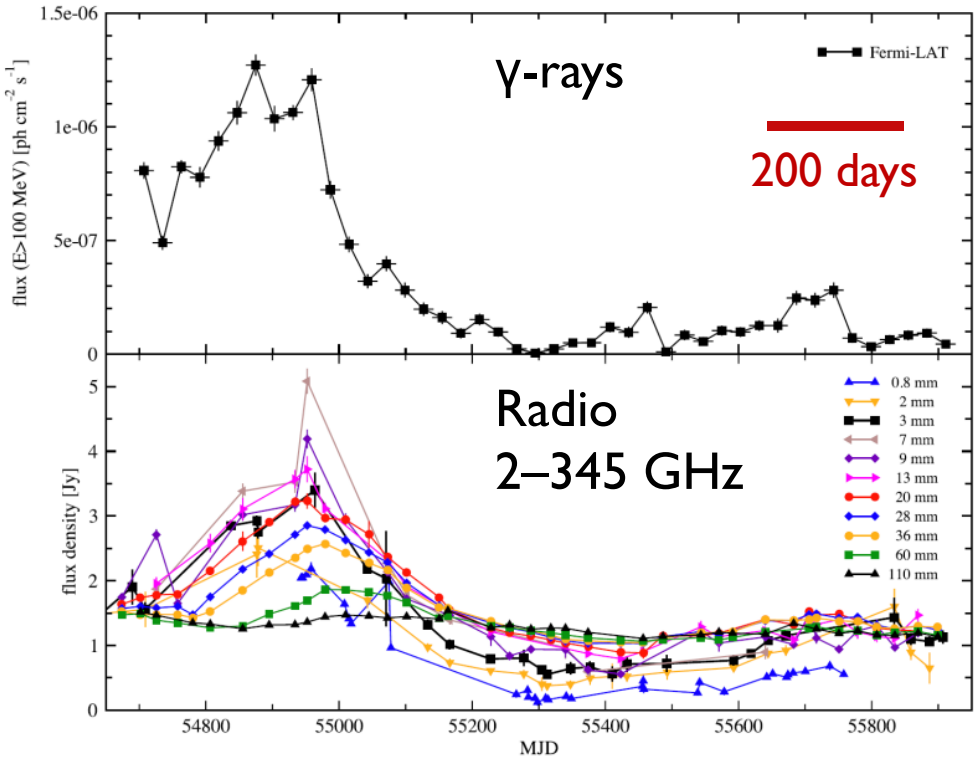

Fuhrmann et al. 2014

Why PKS 1502+106?

- FSRQ with $M_\bullet \approx 10^9\ M_\odot$ at z = 1.839

- Motivation:

  In 2008 *Fermi*/LAT discovered a bright high-energy flare from PKS 1502+106

- followed by delayed radio emission

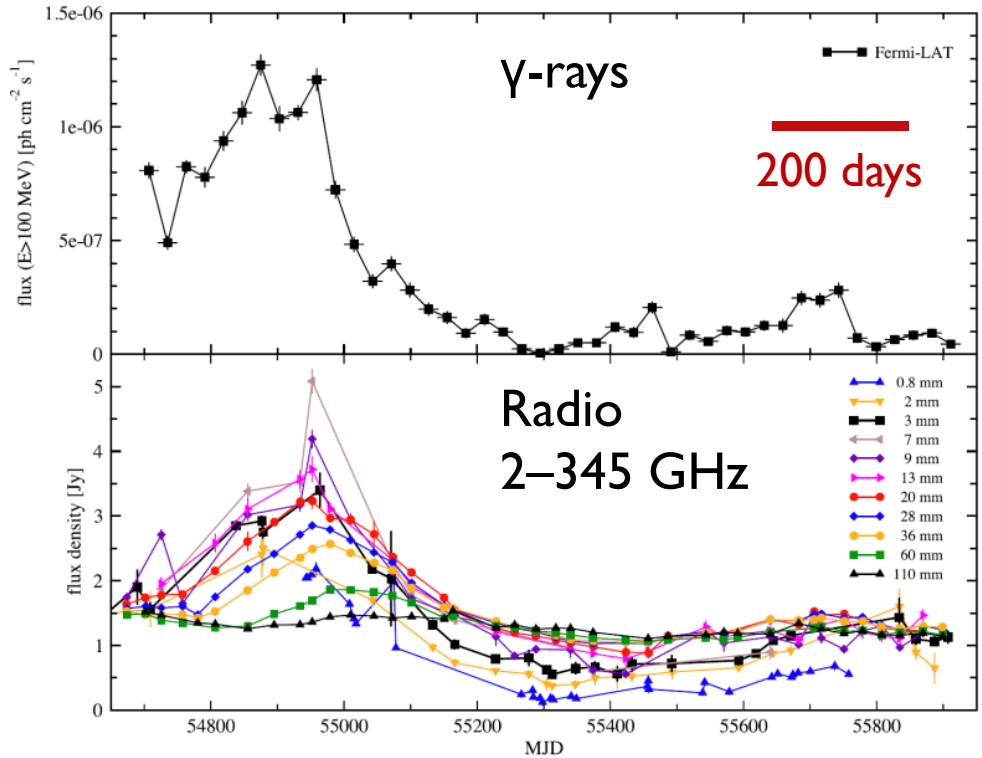

Fuhrmann et al. 2014

Opportunity:

Jet physics (esp. γ-ray emission mechanism) of a distant blazar after a prominent γ-ray flare

What is addressed here and how?

1. Spatial localization of the γ-ray emission region

What is addressed here and how?

1. Spatial localization of the γ-ray emission region
2. Constraining the seed photon field for EC
   - Accretion disk
   - BLR photons
   - IR torus
   - other

What is addressed here and how?

1. Spatial localization of the γ-ray emission region

2. Constraining the seed photon field for EC
   - Accretion disk
   - BLR photons
   - IR torus
   - other …

By combining VLBI
and
single-dish data at multiple frequencies

PKS 1502+106 in its finest detail

- 15 GHz
  - 19 observing epochs between 2002–2011
  - VLBA
  - MOJAVE program (Lister et al. 2009)
- 43 GHz
  - 6 epochs (2009–2012)
  - VLBA
- 86 GHz
  - 6 epochs (2009–2012)
  - GMVA (VLBA + European stations)
  - Simultaneous with 43 GHz

PKS 1502+106 in its finest detail

- 15 GHz
  - 19 observing epochs between 2002–2011
  - VLBA
  - MOJAVE program (Lister et al. 2009)
- 43 GHz
  - 6 epochs (2009–2012)
  - VLBA
- 86 GHz
  - 6 epochs (2009–2012)
  - GMVA (VLBA + European stations)
  - Simultaneous with 43 GHz

1mas = 8.5 pc

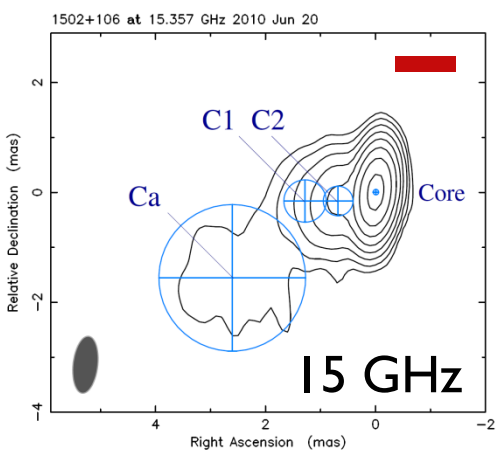

2010.47

15 GHz: (0.15%–19.2%) x 2.8 Jy/b

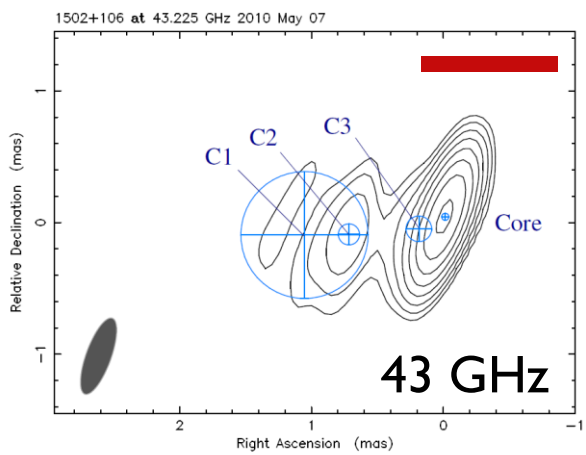

2010.34

43 GHz: (0.1%–12.8%) x 3.5 Jy/b

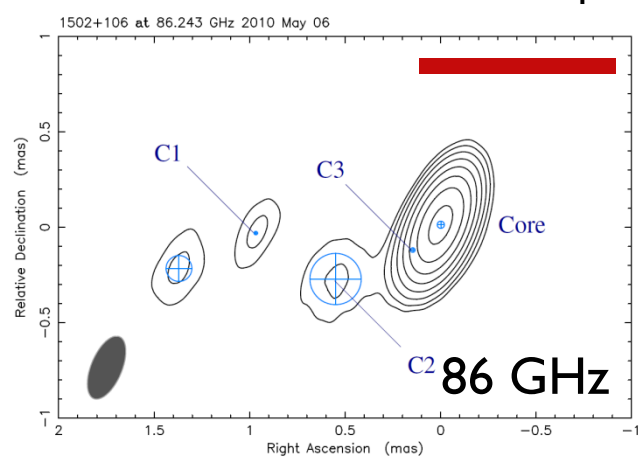

2010.34

86 GHz: (0.15%–19.2%) x 2.2 Jy/b

PKS 1502+106 in its finest detail

- One-sided core–jet morphology
- Bent jet at pc-scales
- Component ejections: 2002–2008.3

1mas = 8.5 pc

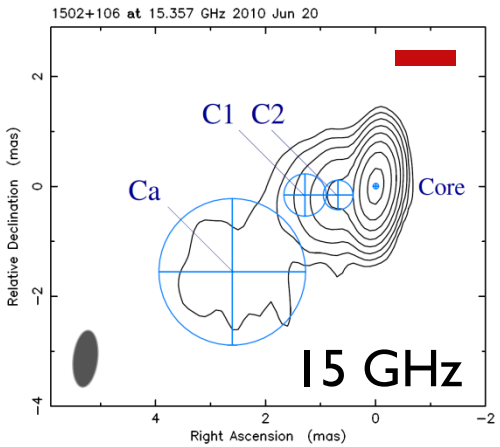

2010.47

15 GHz: (0.15%–19.2%) x 2.8 Jy/b

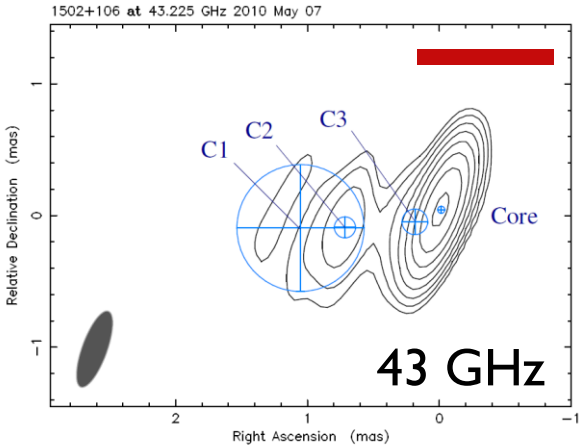

2010.34

43 GHz: (0.1%–12.8%) x 3.5 Jy/b

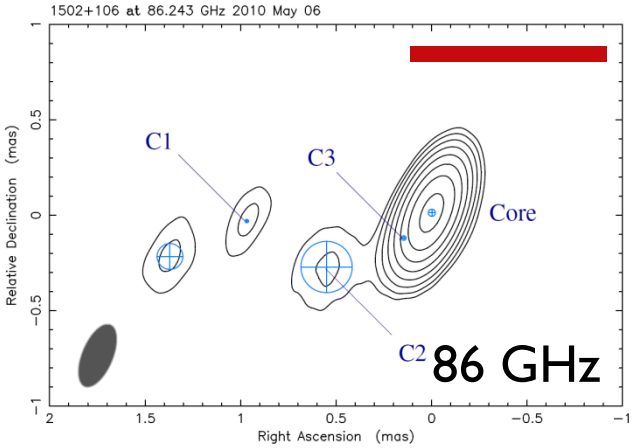

2010.34

86 GHz: (0.15%–19.2%) x 2.2 Jy/b

PKS 1502+106 in its finest detail

- One-sided core–jet morphology
- Bent jet at pc-scales
- Component ejections: 2002–2008.3
- 3 knots cross-identified travelling in different parts of the jet
  - With C3 seen only at 43 and 86 GHz

C1 C2 C3

1mas = 8.5 pc

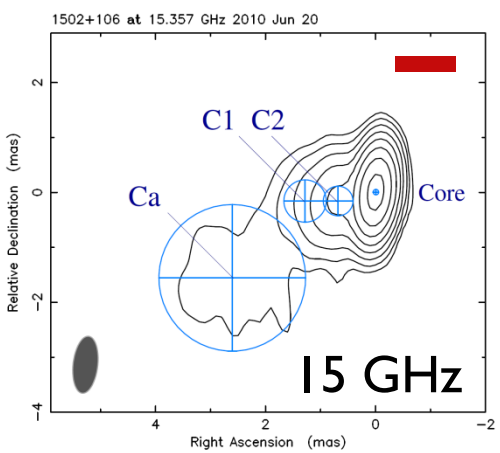

2010.47

15 GHz: (0.15%–19.2%) x 2.8 Jy/b

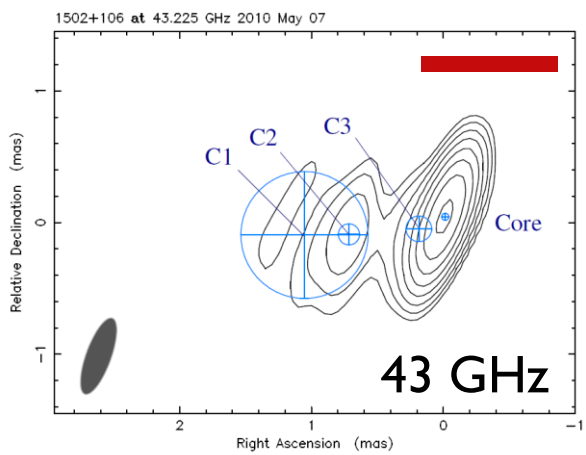

2010.34

43 GHz: (0.1%–12.8%) x 3.5 Jy/b

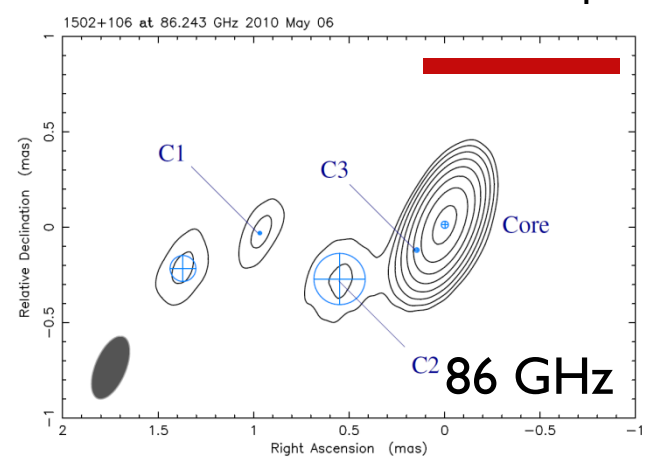

2010.34

86 GHz: (0.15%–19.2%) x 2.2 Jy/b

PKS 1502+106 in its finest detail

1mas = 8.5 pc

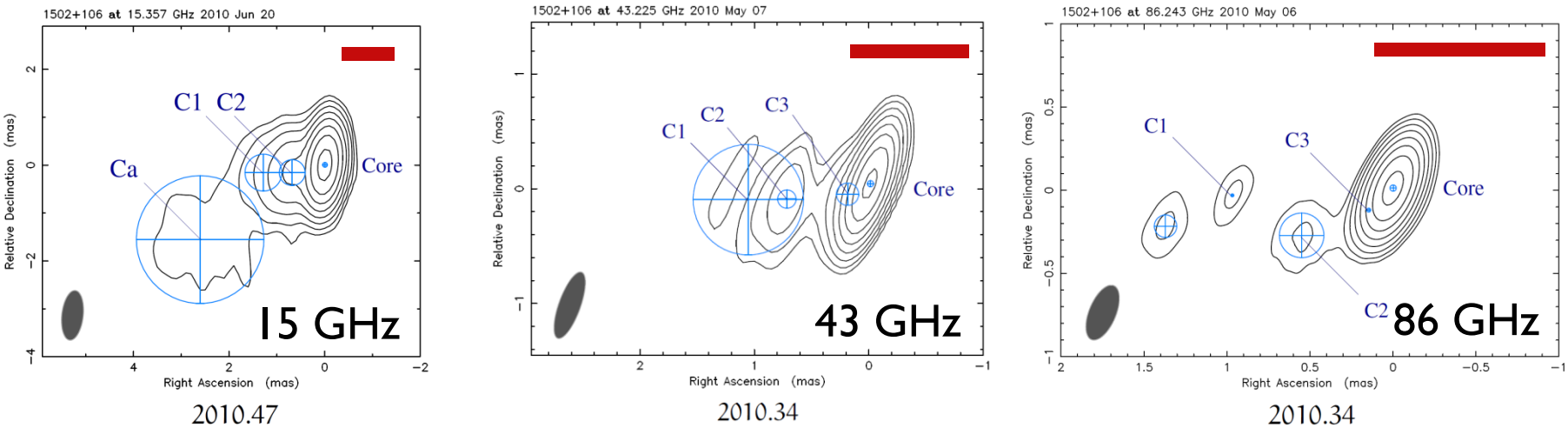

β_{app} & t_{ej}

C1 (22c, 2002)

C2 (9c, 2006)

C3 (7c, 2008.3)

Karamanavis et al. 2016a

PKS 1502+106 in its finest detail

1mas = 8.5 pc

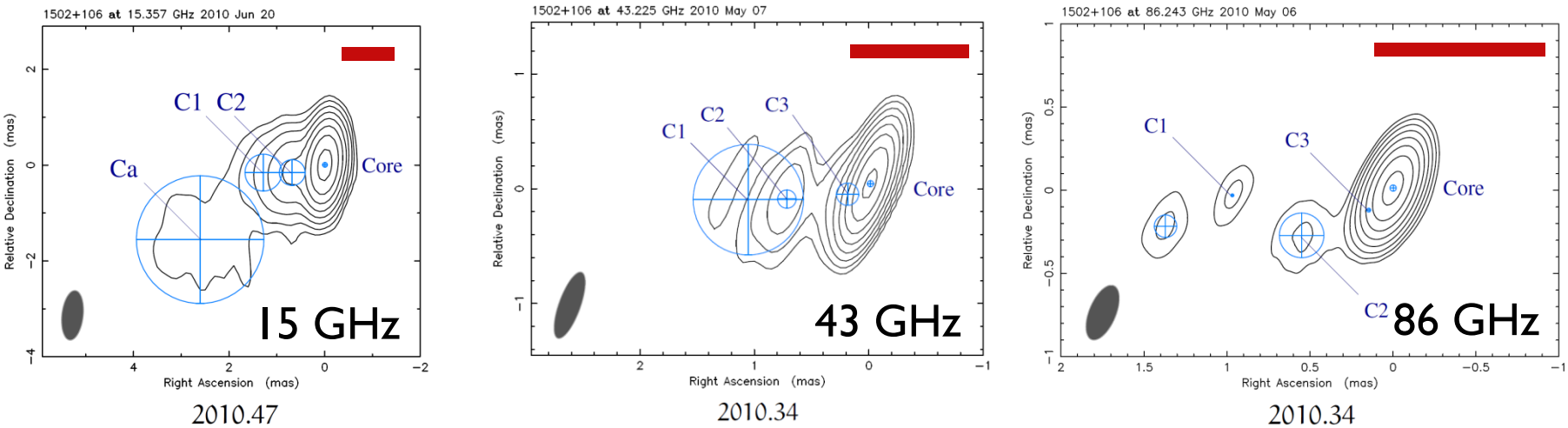

β_{app} & t_{ej}

C1 (22c, 2002)

C2 (9c, 2006)

C3 (7c, 2008.3)

δ

(i) Kinematics, (ii) Variability (Jorstad et al. 2005), and (iii) Magnetic field from SSA (Marscher 1983) and Equipartition (e.g. Bach et al. 2005)

C1 (22c, 2002, δ = 22–50)

C3 (7c, 2008.3, δ = 7–13)

Karamanavis et al. 2016a

What only mm-VLBI can do!

Flux density evolution of jet features

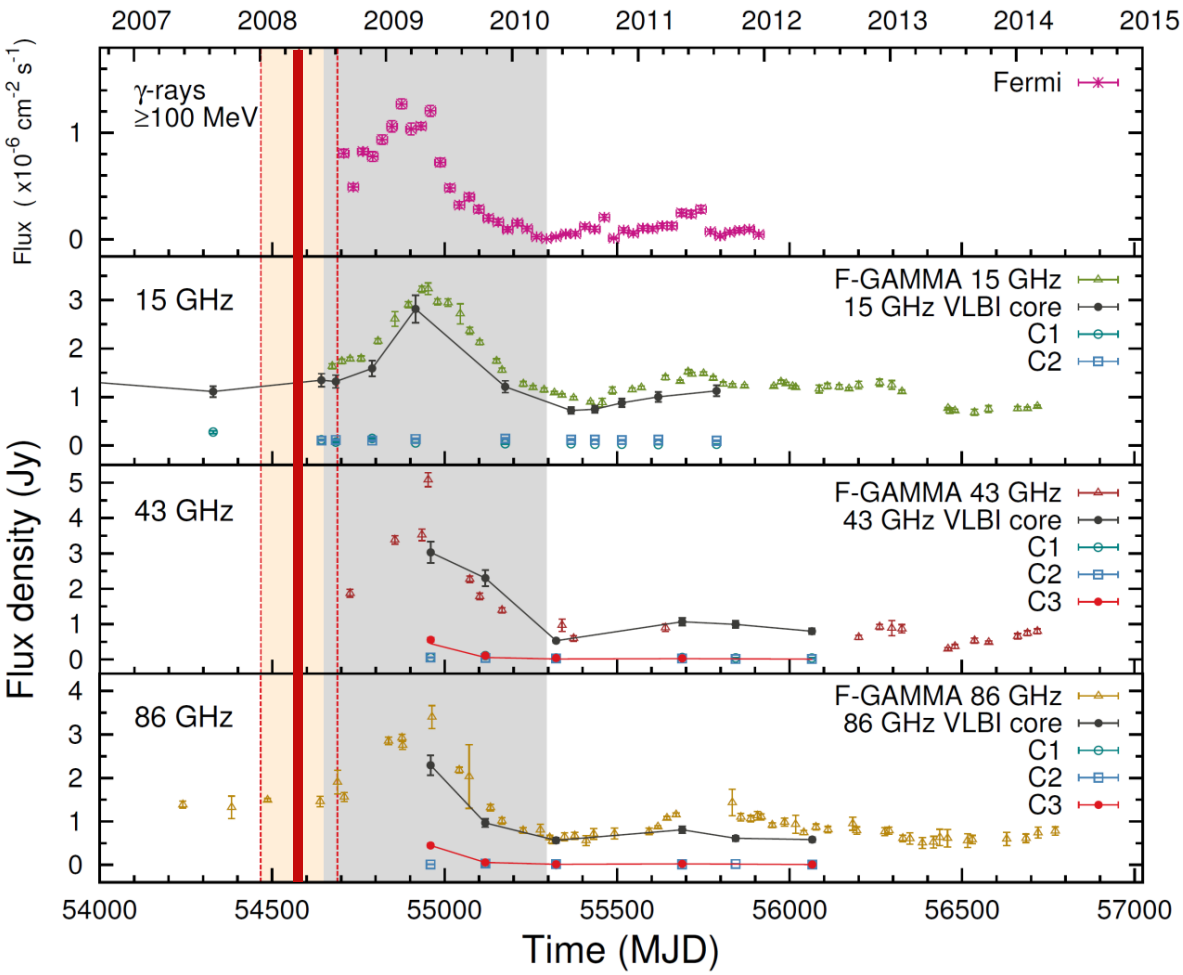

Gray area: Full flare duration
Red line: Ejection time of C3 ± uncertainty

What only mm-VLBI can do!

Flux density evolution of jet features

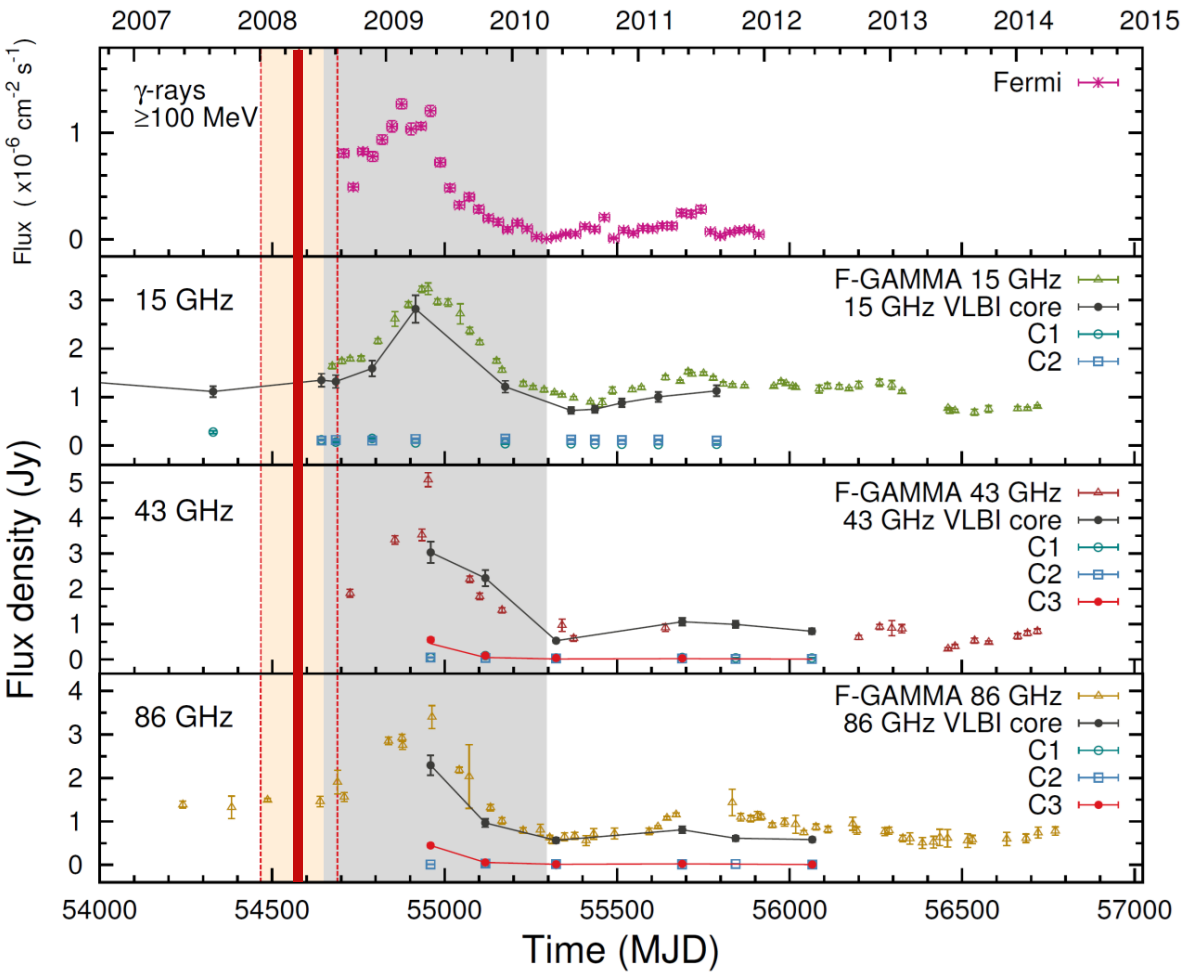

- Core and C3 drive the flare (C3 in decaying phase)

Gray area: Full flare duration
Red line: Ejection time of C3 ± uncertainty

What only mm-VLBI can do!

Flux density evolution of jet features

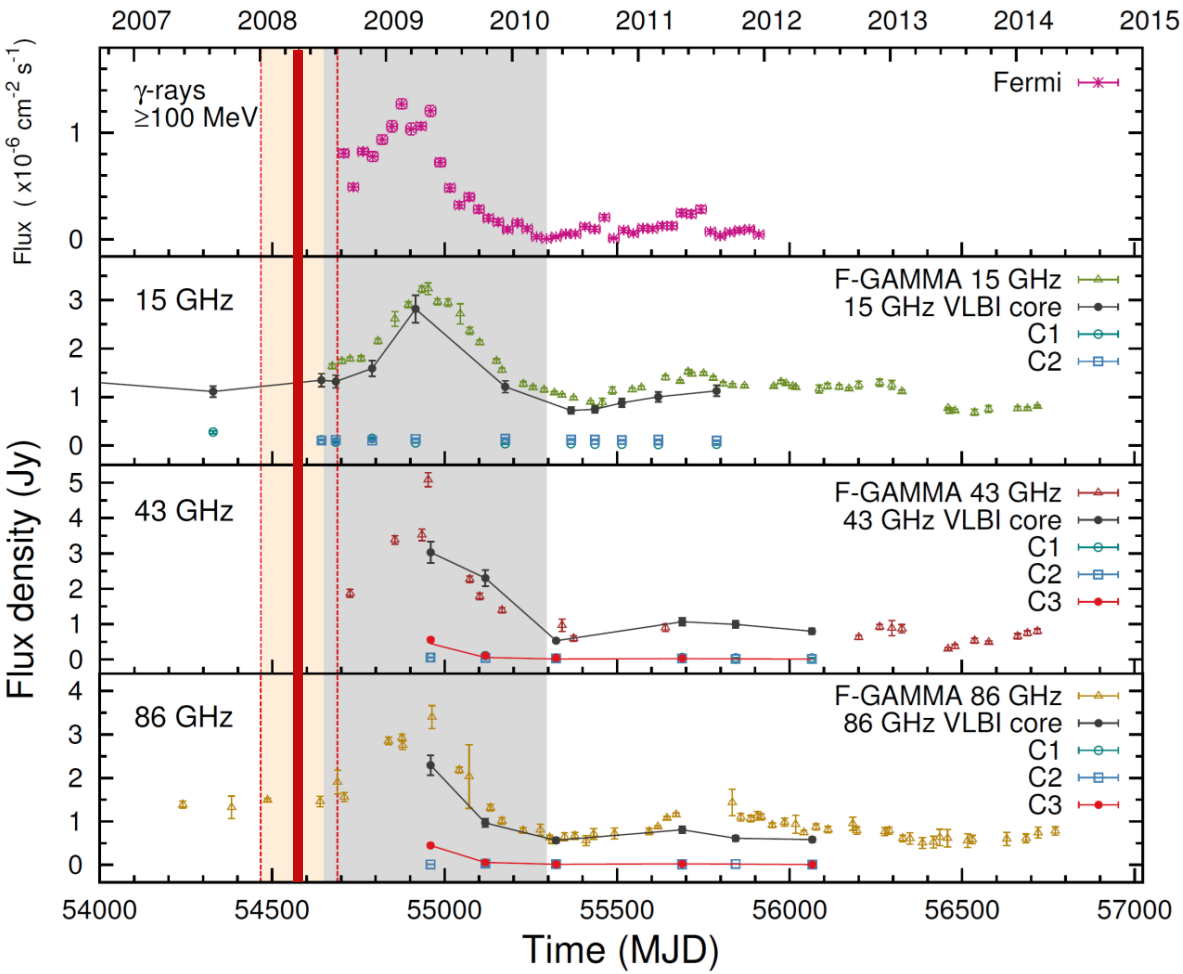

➢ Core and C3 drive the flare (C3 in decaying phase)

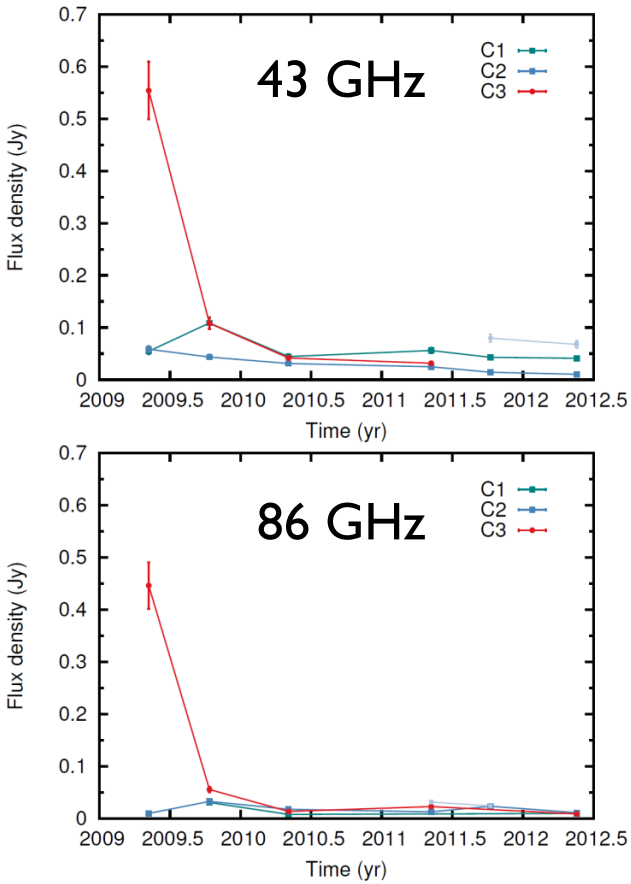

Gray area: Full flare duration
Red line: Ejection time of C3 ± uncertainty

What only mm-VLBI can do!

Flux density evolution of jet features

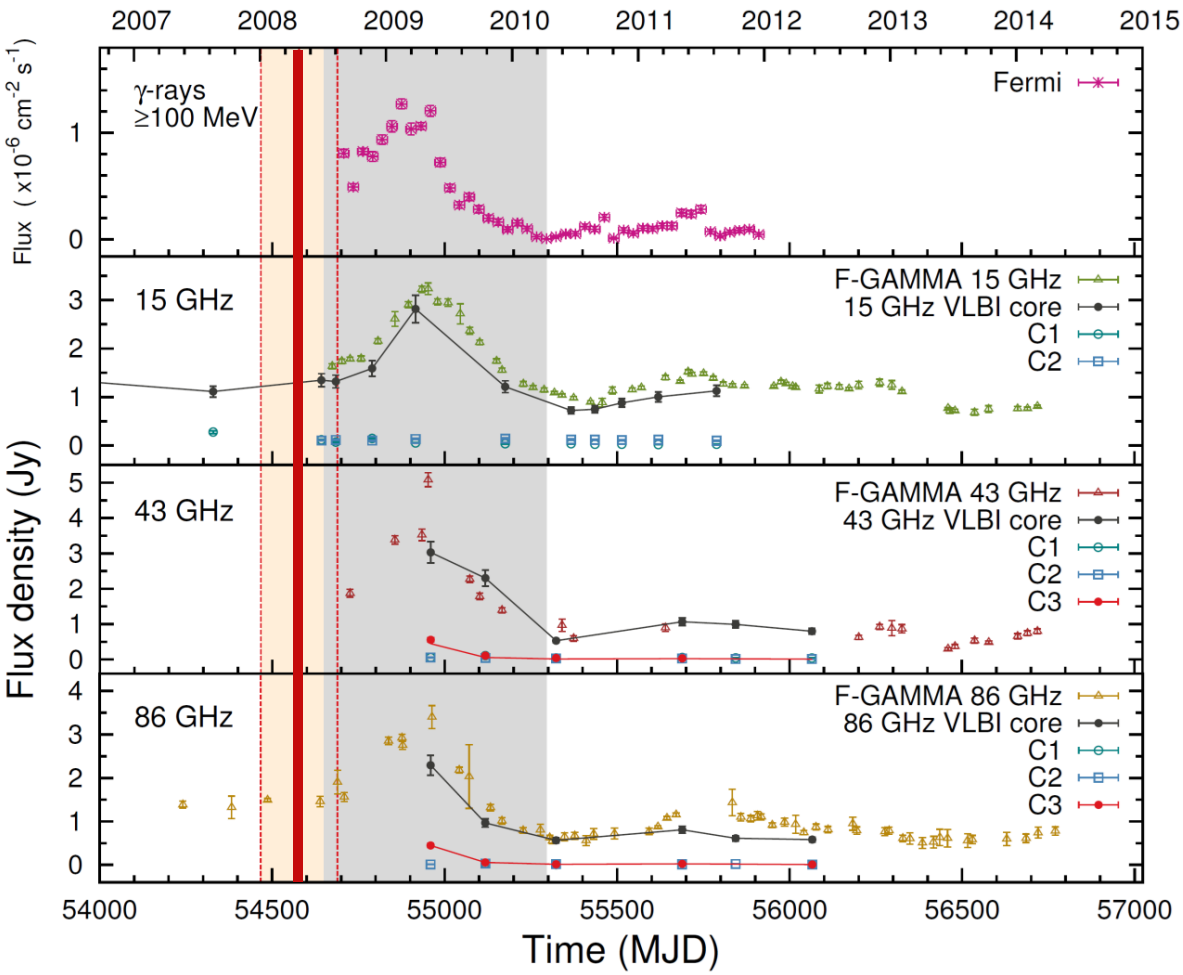

- Core and C3 drive the flare (C3 in decaying phase)
- C3's ejection time coincides with the onset of γ-ray activity and
- Only C3 can be associated with the flare

Gray area: Full flare duration
Red line: Ejection time of C3 ± uncertainty

Single-dish add-ons

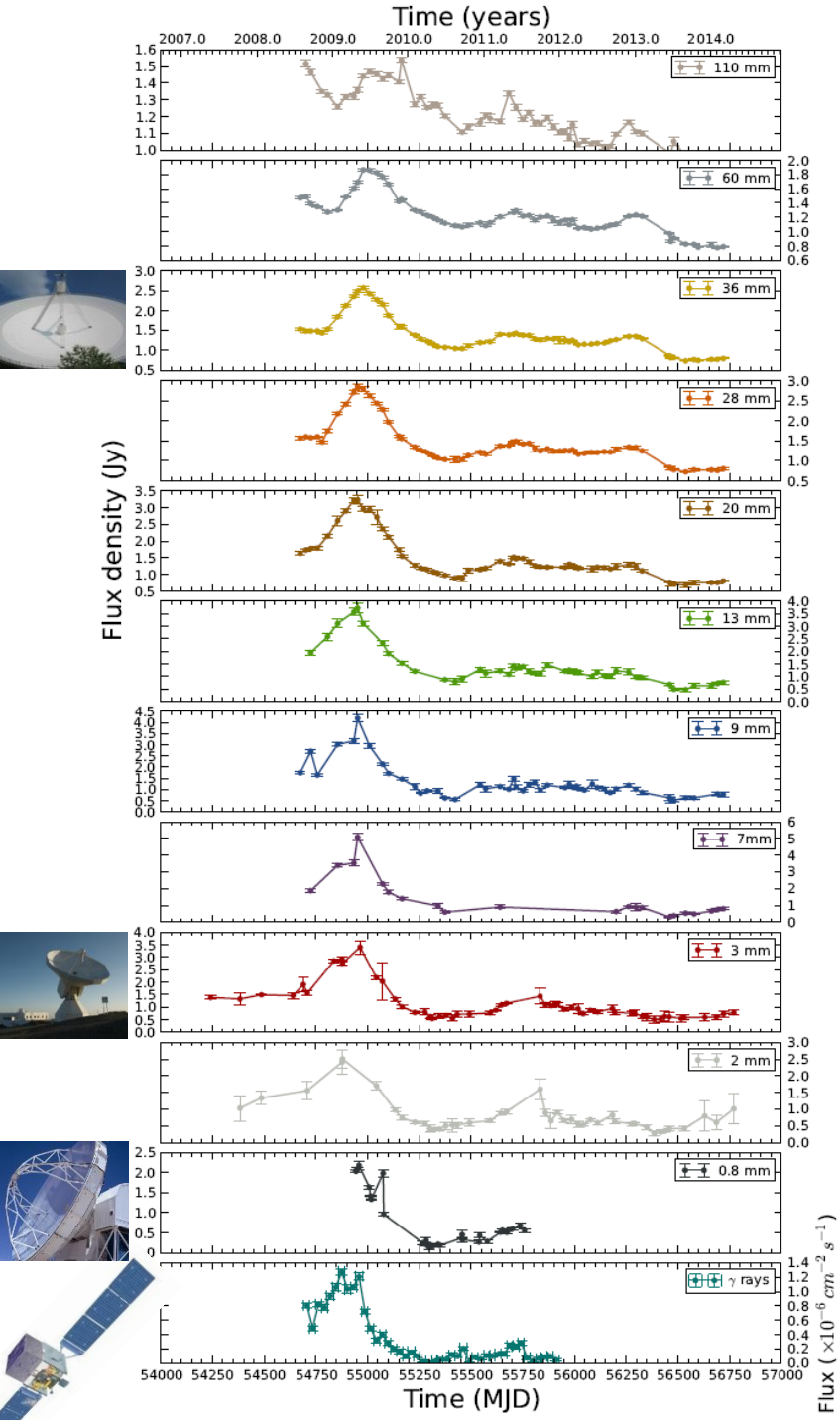

2.64

4.85

8.35 GHz

10.45

14.60

23.05

32.00

43.00

86.24

142.33

345.00

γ-rays>100MeV

F-GAMMA program

(Fuhrmann et al. 2016)

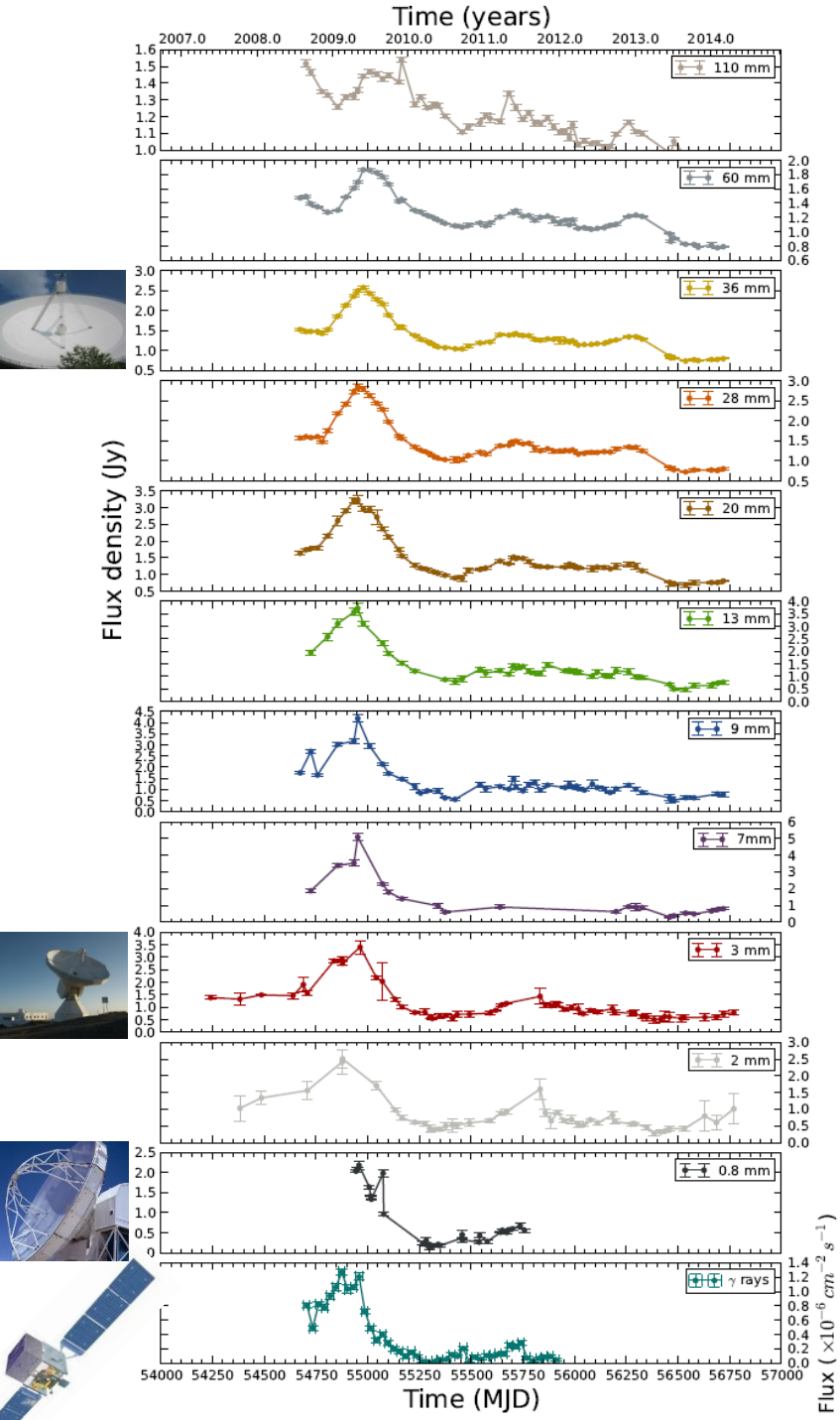

2.64

4.85

8.35 GHz

10.45

14.60

23.05

32.00

43.00

86.24

142.33

345.00

γ-rays>100MeV

Extraction of parameters:

- Flare amplitude,
- Flare time scales, and
- Time delays of flare maxima at different frequencies (cross-band delays)

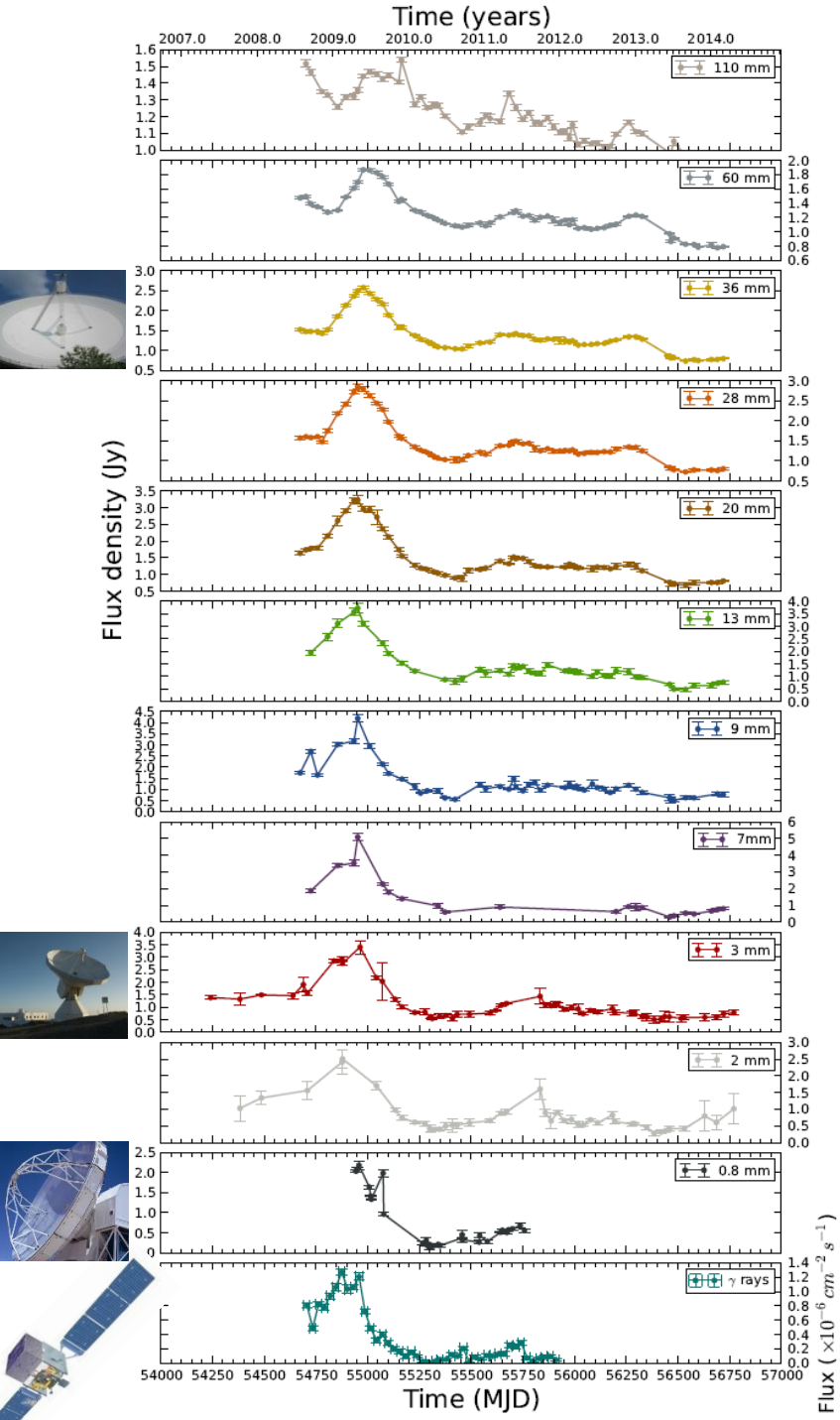

2.64

4.85

8.35 GHz

10.45

14.60

23.05

32.00

43.00

86.24

142.33

345.00

γ-rays>100MeV

Gaussian process regression

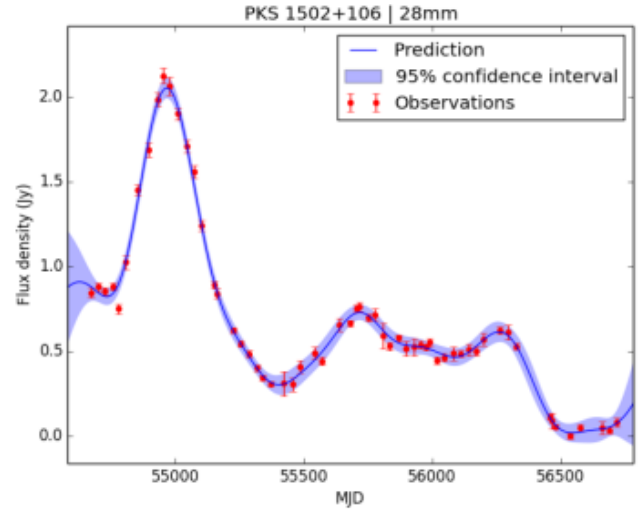

(d) 10.45 GHz

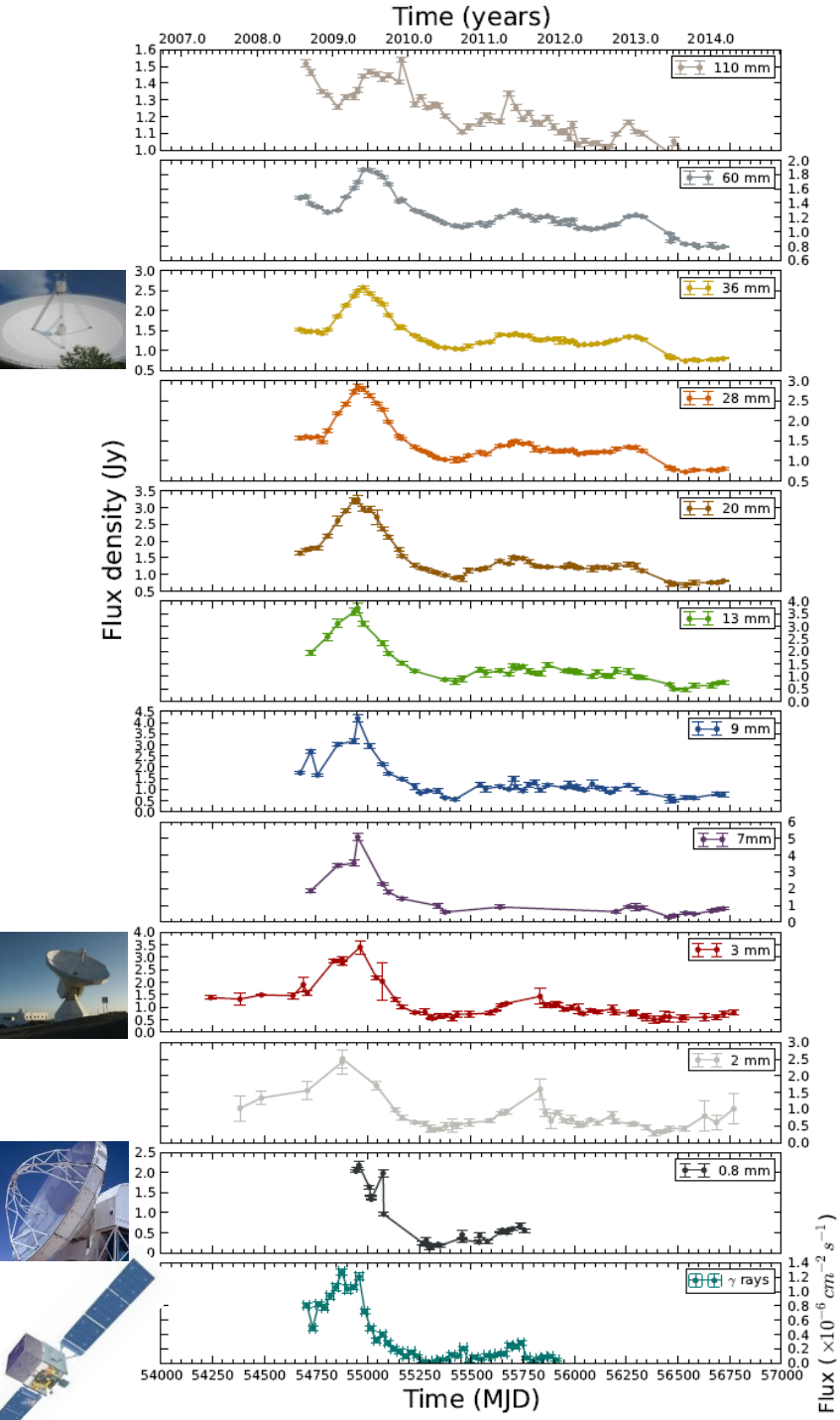

2.64

4.85

8.35 GHz

10.45

14.60

23.05

32.00

43.00

86.24

142.33

345.00

γ-rays>100MeV

Gaussian process regression

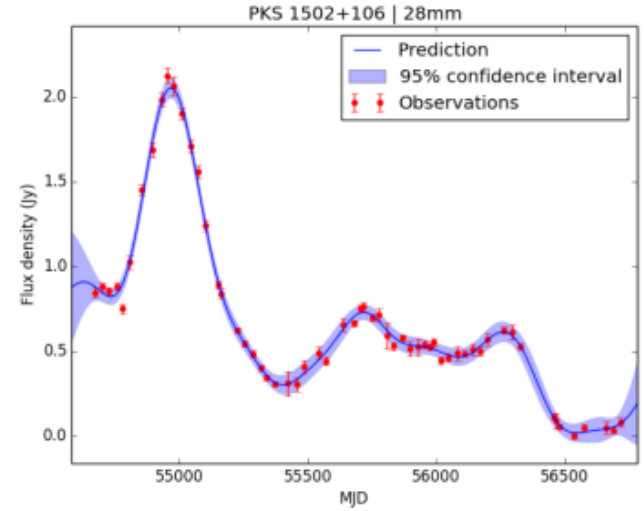

(d) 10.45 GHz

DCCF

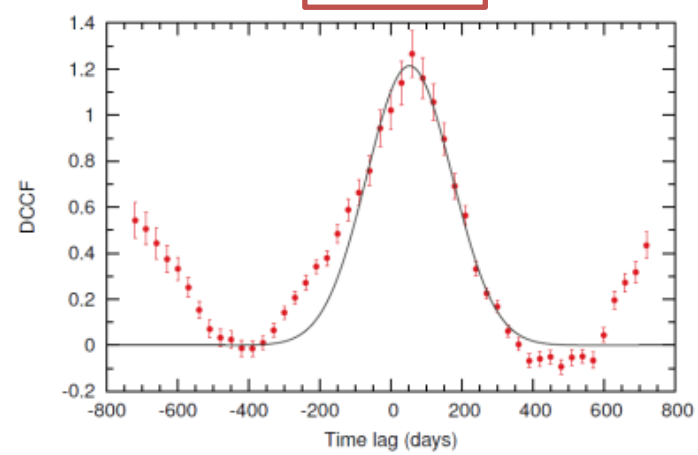

10.45/15.00 GHz

Gaussian processes & regression

Various methods used for light curve fitting:

- Exponential flares
- Gaussian fits
- Other…

Gaussian processes & regression

Various methods used for light curve fitting:

- Exponential flares
- Gaussian fits
- Other…

BUT

parametric models;
i.e. all assume a f(x)

Gaussian processes & regression

Various methods used for light curve fitting:

- Exponential flares
- Gaussian fits
- Other…

BUT

parametric models;
i.e. all assume a f(x)

GPs are generalized Gaussian distributions over functions;
i.e. collection of functions characterized by a mean and a st. dev.

See Rasmusen & Williams 2006

Gaussian processes & regression

Various methods used for light curve fitting:

- Exponential flares
- Gaussian fits
- Other…

BUT

parametric models;
i.e. all assume a f(x)

GPs are generalized Gaussian distributions over functions;
i.e. collection of functions characterized by a mean and a st. dev.

Bayesian prior

See Rasmusen & Williams 2006

Gaussian processes & regression

Various methods used for light curve fitting:

- Exponential flares
- Gaussian fits
- Other…

BUT

parametric models;
i.e. all assume a f(x)

GPs are generalized Gaussian distributions over functions;
i.e. collection of functions characterized by a mean and a st. dev.

Bayesian prior

The only assumption going into them is the covariance kernel that generates them:

$$k(x_i, x_j) = \sigma_f^2 \exp\left[\frac{-(x_i - x_j)^2}{2l^2}\right]$$

Defines the covariance between two f values at x_i and x_j

Maps our prior beliefs for the underlying process

See Rasmusen & Williams 2006

Gaussian processes & regression

Prior distribution

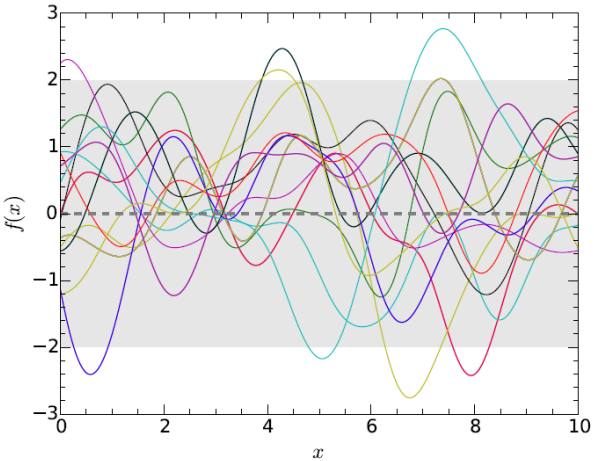

Gaussian processes & regression

Prior distribution

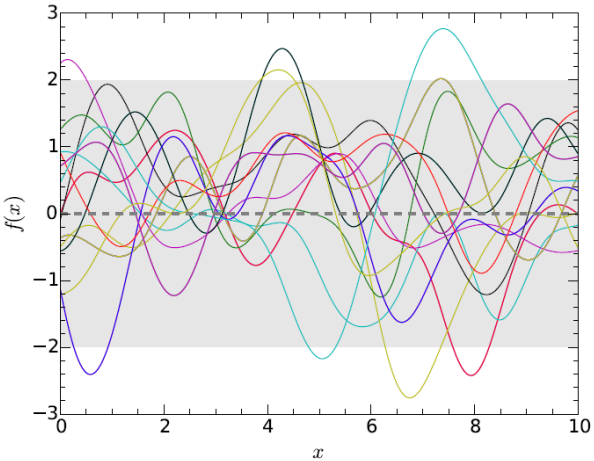

Training on data

We optimize, i.e. select the functions that pass through all observations.

Gaussian processes & regression

Prior distribution

Posterior distribution

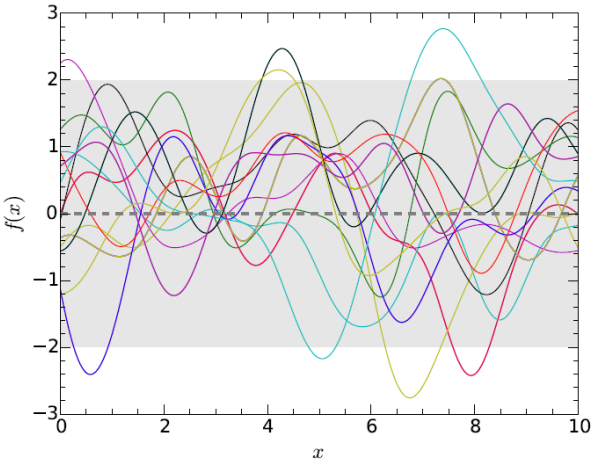

Training on data

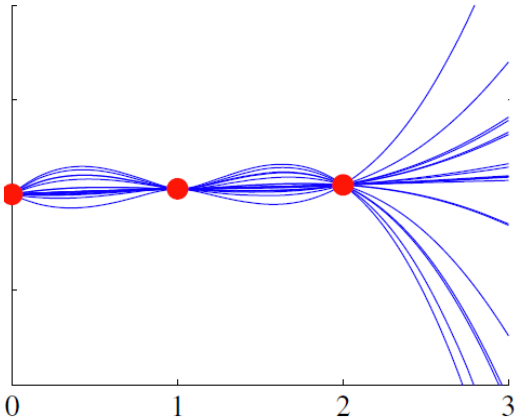

Roberts et al. 2011

We optimize, i.e. select the functions that pass through all observations.

Gaussian processes & regression

Prior distribution

Posterior distribution

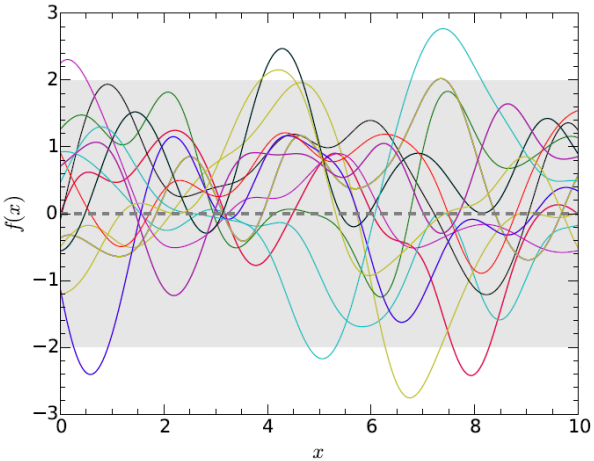

Training on data

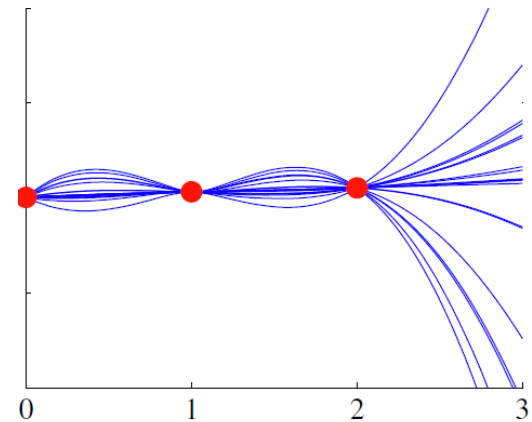

Roberts et al. 2011

We optimize, i.e. select the functions that pass through all observations.

Posterior mean and confidence interval

Gaussian processes & regression

Prior distribution

Posterior distribution

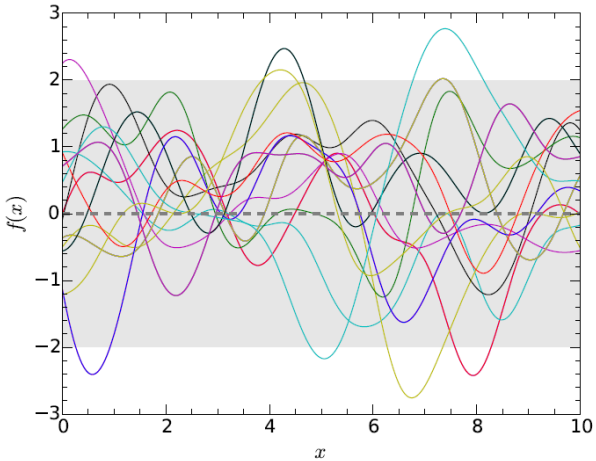

Training on data

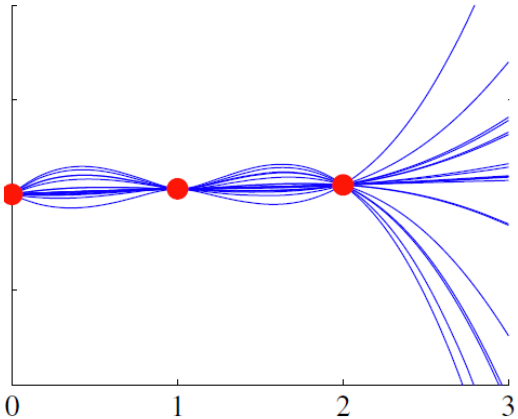

Roberts et al. 2011

We optimize, i.e. select the functions that pass through all observations.

Posterior mean and confidence interval

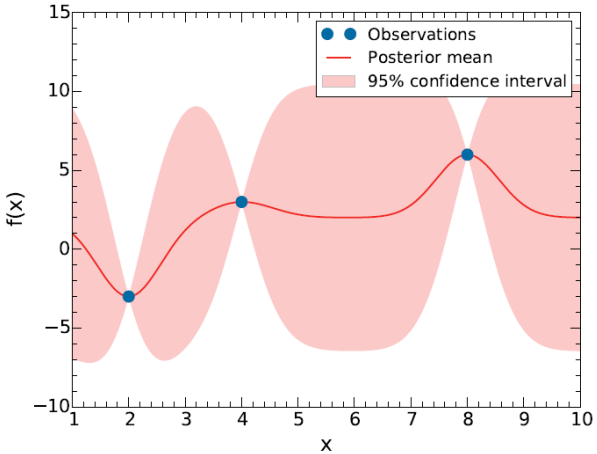

Gaussian processes & regression

Prior distribution

Posterior distribution

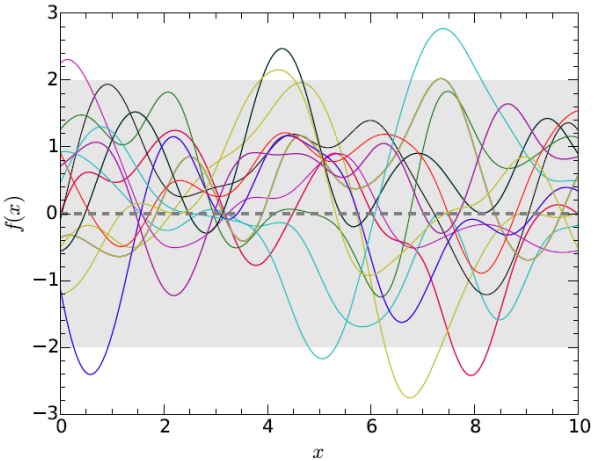

Training on data

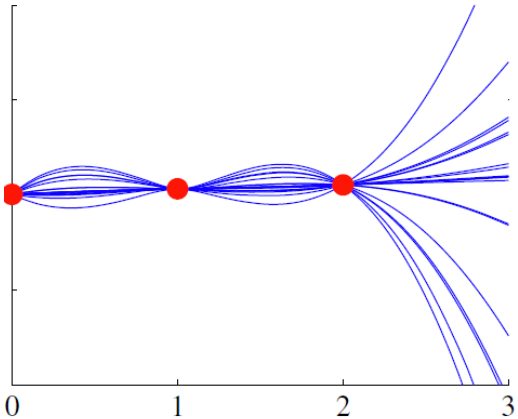

Roberts et al. 2011

We optimize, i.e. select the functions that pass through all observations.

Posterior mean and confidence interval

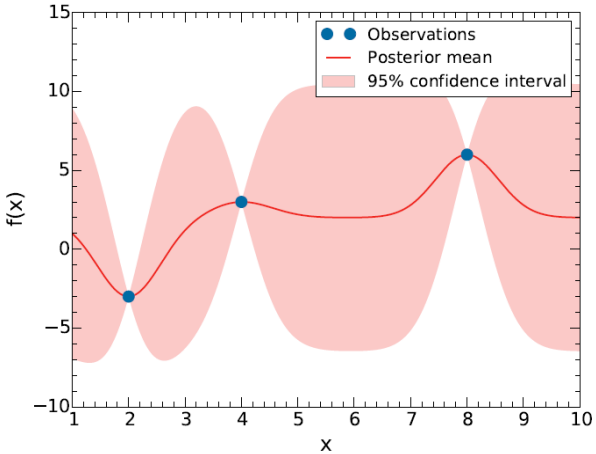

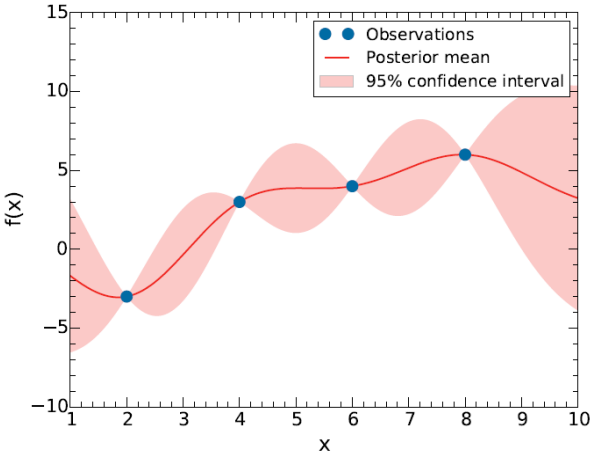

Gaussian processes & regression

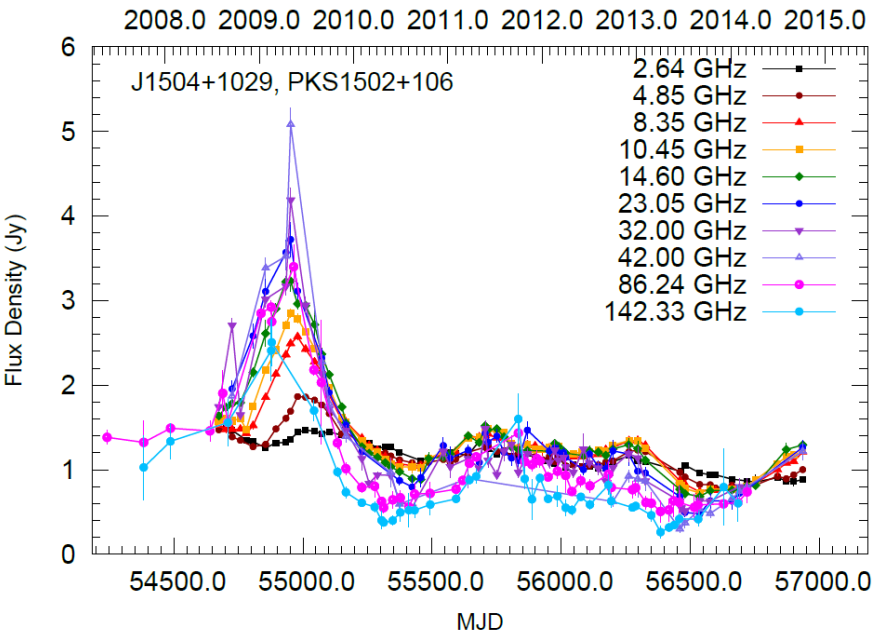

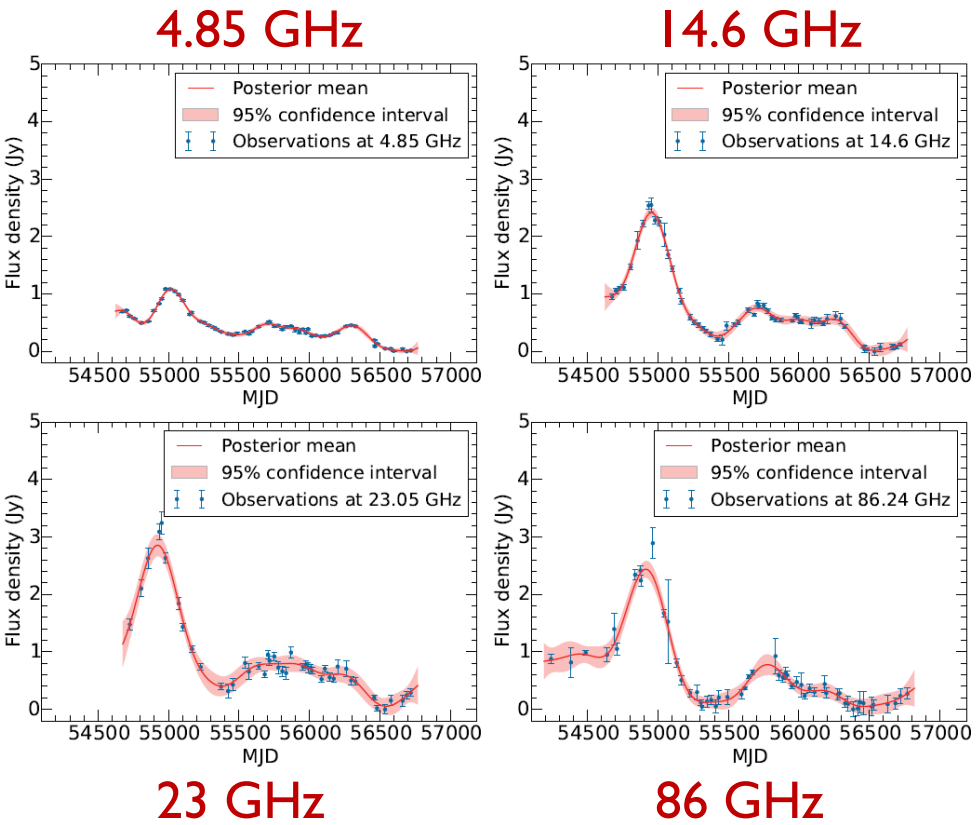

Gaussian processes & regression

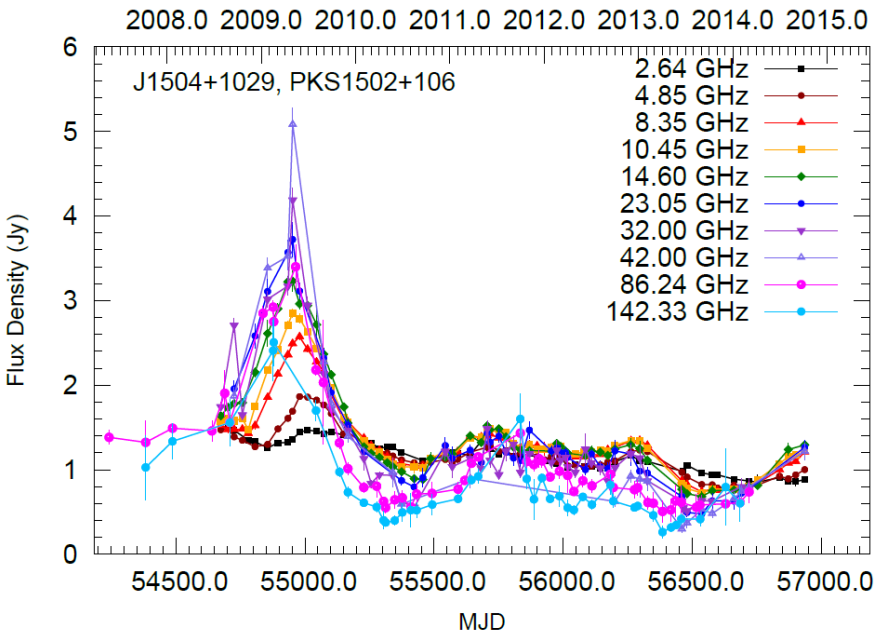

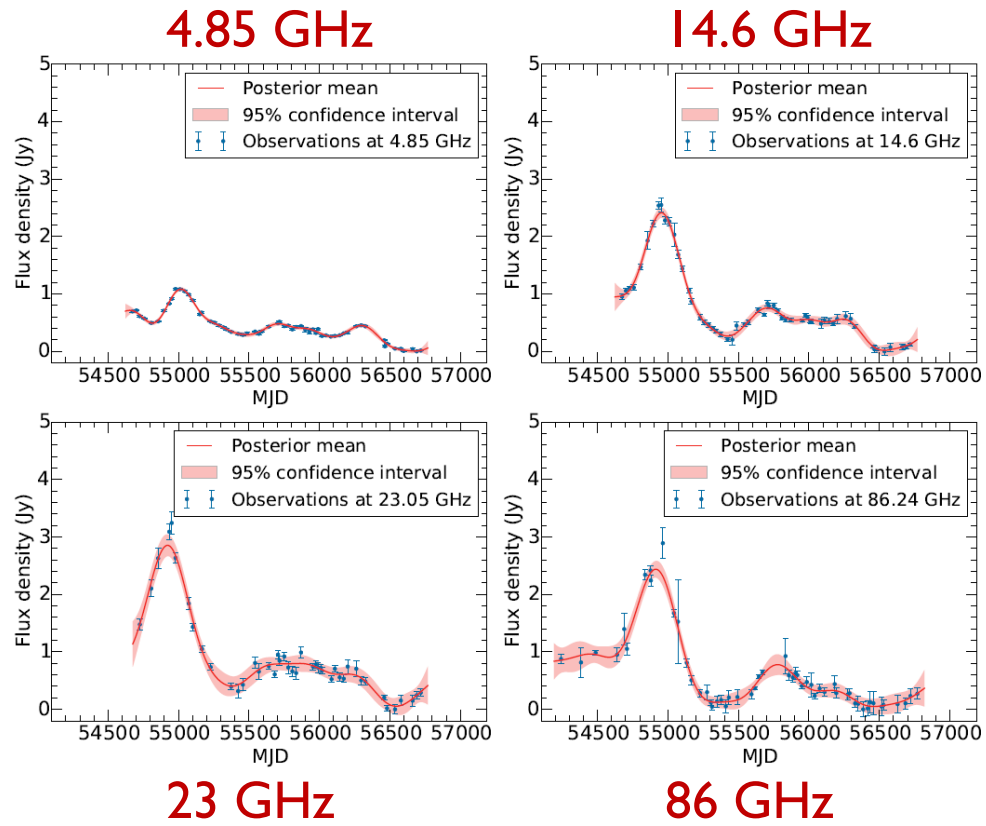

GPs offer:

- An elegant alternative to parametric fitting
- Results generally free of biases
- Very good error estimation
- Vast domain of application (not only blazars!)

Jet nuclear opacity & the HE emission

- Flare maxima show time delays wrt highest frequency

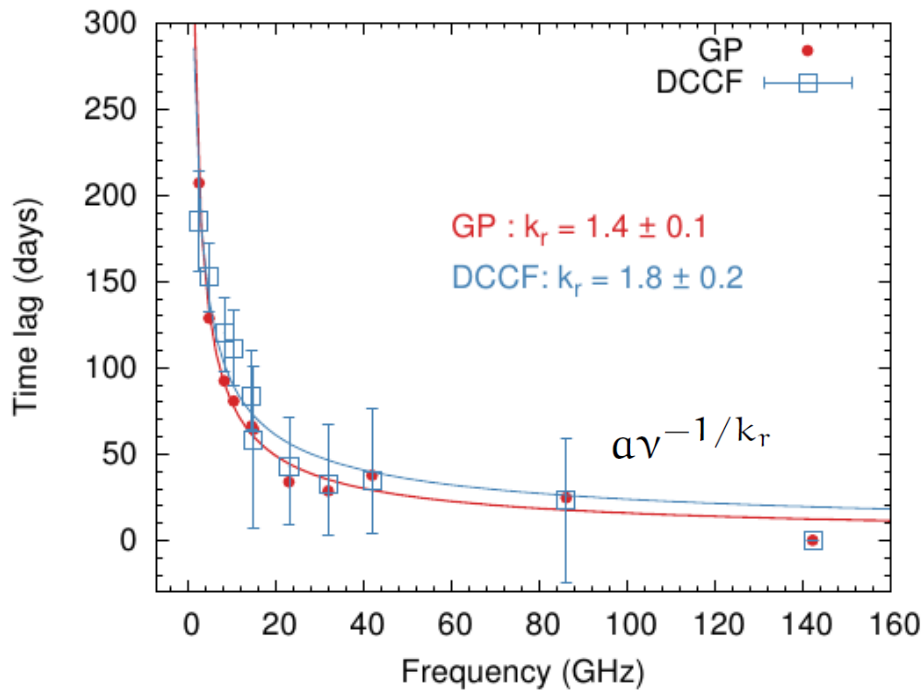

Karamanavis et al. 2016b

Jet nuclear opacity & the HE emission

- Flare maxima show time delays wrt highest frequency
- Due to optical depth; i.e. synchrotron opacity (Lobanov 1998, Hirotani 2005)

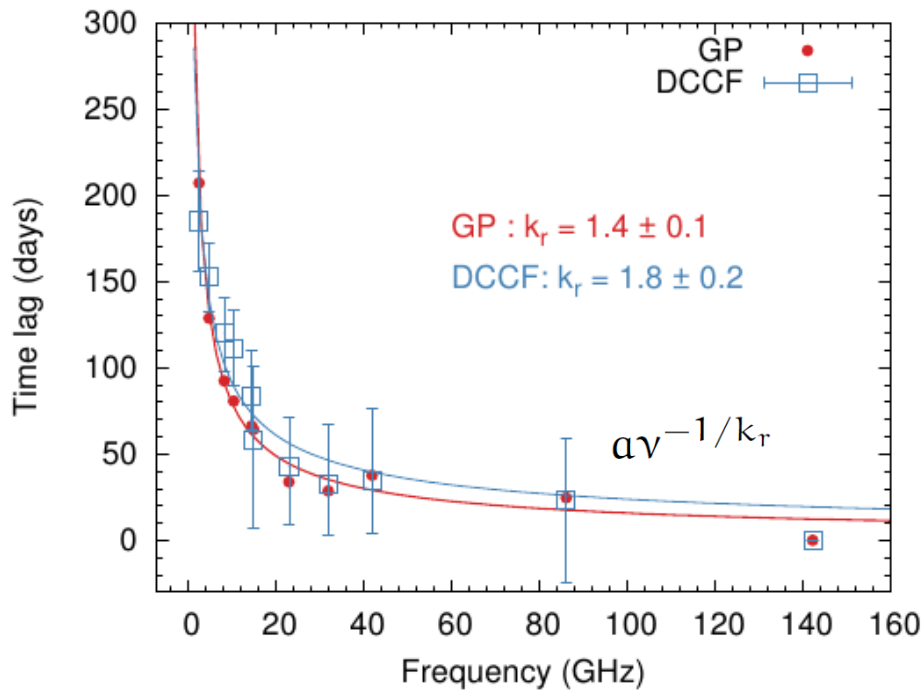

Karamanavis et al. 2016b

Jet nuclear opacity & the HE emission

- Flare maxima show time delays wrt highest frequency
- Due to optical depth; i.e. synchrotron opacity (Lobanov 1998, Hirotani 2005)
- Tomography of the jet in terms of nuclear opacity (VLBI-free core shifts)

  (e.g. Kudryavtseva et al. 2011, Kutkin et al. 2013)

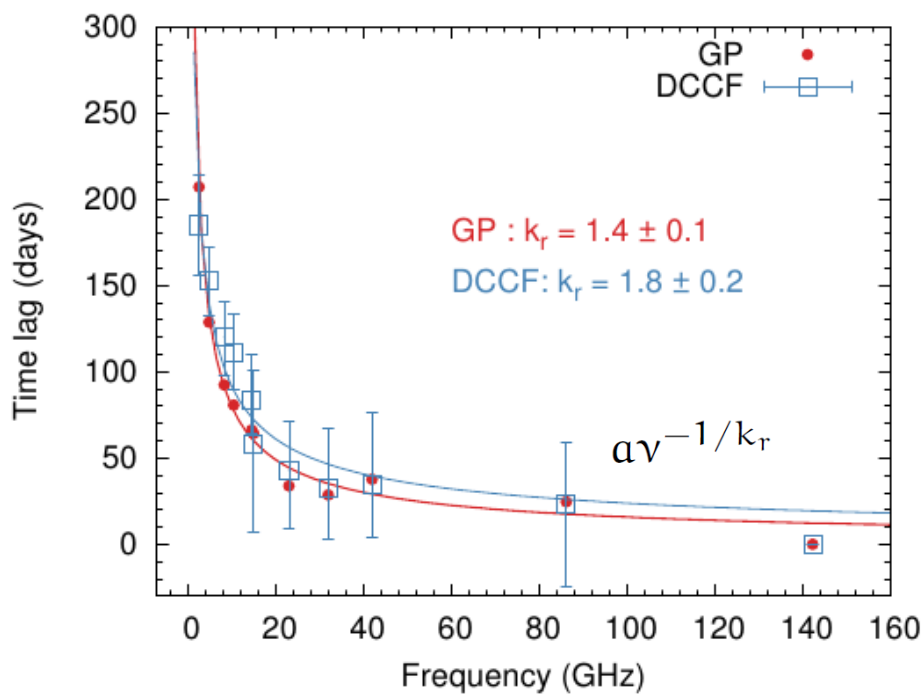

ν (GHz)	r_{core} (pc)
2.64	10.2 ± 1.2
4.85	7.1 ± 1.0
8.35	5.3 ± 0.8
10.45	4.8 ± 0.8
14.60	4.0 ± 0.7
15.00	3.8 ± 0.7
23.05	2.6 ± 0.6
32.00	2.9 ± 1.0
43.05	3.4 ± 0.8
86.24	4.0 ± 1.1

Karamanavis et al. 2016b

Jet nuclear opacity & the HE emission

- Flare maxima show time delays wrt highest frequency
- Due to optical depth; i.e. synchrotron opacity (Lobanov 1998, Hirotani 2005)
- Tomography of the jet in terms of nuclear opacity (VLBI-free core shifts)

  (e.g. Kudryavtseva et al. 2011, Kutkin et al. 2013)

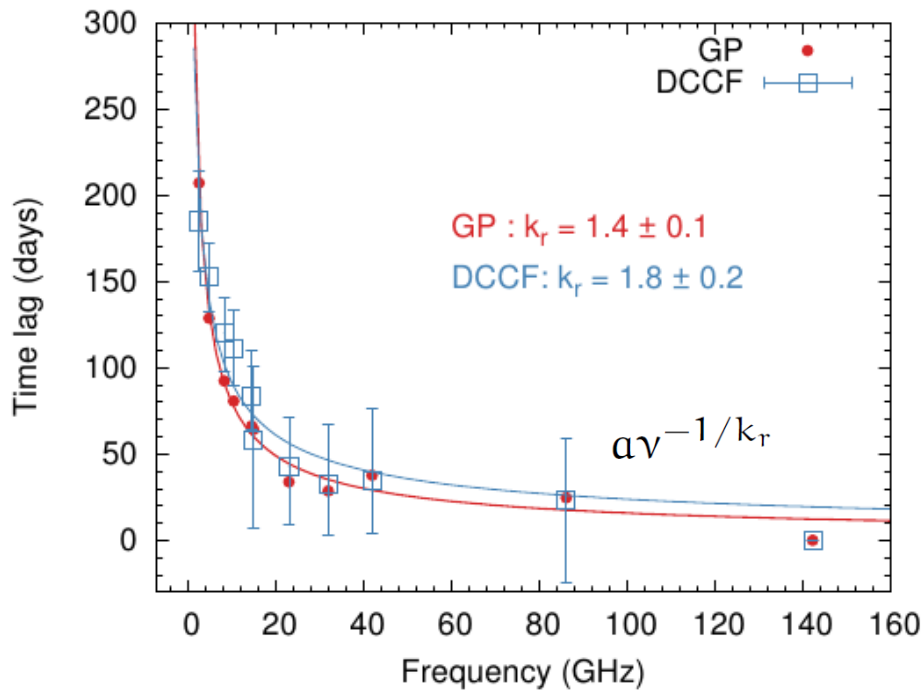

ν (GHz)	r_{core} (pc)
2.64	10.2 ± 1.2
4.85	7.1 ± 1.0
8.35	5.3 ± 0.8
10.45	4.8 ± 0.8
14.60	4.0 ± 0.7
15.00	3.8 ± 0.7
23.05	2.6 ± 0.6
32.00	2.9 ± 1.0
43.05	3.4 ± 0.8
86.24	4.0 ± 1.1

Karamanavis et al. 2016b

Jet nuclear opacity & the HE emission

- Flare maxima show time delays wrt highest frequency
- Due to optical depth; i.e. synchrotron opacity (Lobanov 1998, Hirotani 2005)
- Tomography of the jet in terms of nuclear opacity (VLBI-free core shifts) (e.g. Kudryavtseva et al. 2011, Kutkin et al. 2013)

- Relative distance between the 3mm core and HE site (Fuhrmann et al. 2014)

Karamanavis et al. 2016b

Jet nuclear opacity & the HE emission

- Flare maxima show time delays wrt highest frequency
- Due to optical depth; i.e. synchrotron opacity (Lobanov 1998, Hirotani 2005)
- Tomography of the jet in terms of nuclear opacity (VLBI-free core shifts) (e.g. Kudryavtseva et al. 2011, Kutkin et al. 2013)

- Relative distance between the 3mm core and HE site (Fuhrmann et al. 2014)
- With our absolute distance of the 3mm core from the jet base (~4 pc)

Karamanavis et al. 2016b

Jet nuclear opacity & the HE emission

- Flare maxima show time delays wrt highest frequency
- Due to optical depth; i.e. synchrotron opacity (Lobanov 1998, Hirotani 2005)
- Tomography of the jet in terms of nuclear opacity (VLBI-free core shifts) (e.g. Kudryavtseva et al. 2011, Kutkin et al. 2013)

- Relative distance between the 3mm core and HE site (Fuhrmann et al. 2014)
- With our absolute distance of the 3mm core from the jet base (~4 pc)
- Managed to constrain the site of HE emission to about 2 pc from the base

Karamanavis et al. 2016b

Jet nuclear opacity & the HE emission

- Flare maxima show time delays wrt highest frequency
- Due to optical depth; i.e. synchrotron opacity (Lobanov 1998, Hirotani 2005)
- Tomography of the jet in terms of nuclear opacity (VLBI-free core shifts) (e.g. Kudryavtseva et al. 2011, Kutkin et al. 2013)

- Relative distance between the 3mm core and HE site (Fuhrmann et al. 2014)
- With our absolute distance of the 3mm core from the jet base (~4 pc)
- Managed to constrain the site of HE emission to about 2 pc from the base
  - Important: BLR radius for PKS 1502+106 = 0.1 pc (Abdo et al. 2010)
  - BLR photon field too dilute [$n(R) \propto 1/R$; Poutanen & Stern (2010)]

Karamanavis et al. 2016b

Conclusions

1. mm-VLBI allowed us to pinpoint the component connected with the intense gamma-ray flare from PKS 1502+106 (C3)

Conclusions

1. mm-VLBI allowed us to pinpoint the component connected with the intense gamma-ray flare from PKS 1502+106 (C3)

2. High-energy emission originates from a region ~2 pc away from the jet base.

Conclusions

1. mm-VLBI allowed us to pinpoint the component connected with the intense gamma-ray flare from PKS 1502+106 (C3)

2. High-energy emission originates from a region ~2 pc away from the jet base.

3. We can readily exclude accretion disk and Broad-Line Region (BLR) photons as targets for External Compton (ERC)

Conclusions

1. mm-VLBI allowed us to pinpoint the component connected with the intense gamma-ray flare from PKS 1502+106

2. High-energy emission originates from a region ~2 pc away from the jet base.

3. We can readily exclude accretion disk and Broad-Line Region (BLR) photons as targets for External Compton (ERC)

4. Photon field of the IR torus could play a role here
   - In addition to the Synchrotron Self-Compton (SSC) mechanism

Thank you!

Lots of hidden slides

Doppler and Lorentz factors

1. Kinematics $\gamma_{\rm min} = \sqrt{\beta_{\rm app}^2 + 1}$ (e.g. Urry & Padovani 1995)
   1. C1: $\delta_{min} \approx \gamma_{min} \approx 22$
   2. C2: $\delta_{min} \approx \gamma_{min} \approx 9$
   3. C3: $\delta_{min} \approx \gamma_{min} \approx 7$

2. Variability of components (causality arguments and size of the emitting region) (Jorstad et al. 2005)
   1. C1: $\delta_{var} \leq 52$ and $\gamma_{var} \leq 31$ (15 GHz)
   2. C3: $\delta_{var} \leq 12–15$ and $\gamma_{var} \leq 7–9$ (43 & 86 GHz)

3. Magnetic field from SSA (Marscher 1983) and Equipartition (e.g. Bach et al. 2005)

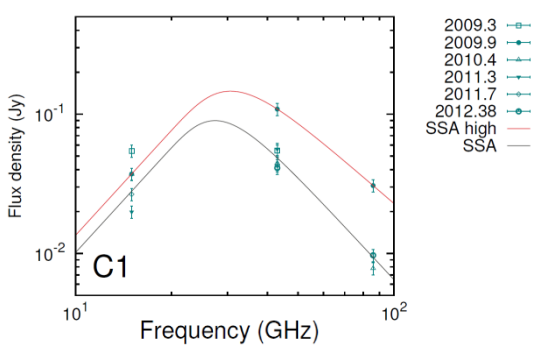

$$B_{eq}/B_{SSA} = \delta_{eq}^{2/7\alpha}.$$

– C1: $\delta_{eq} \approx 50$

Intrinsic jet properties

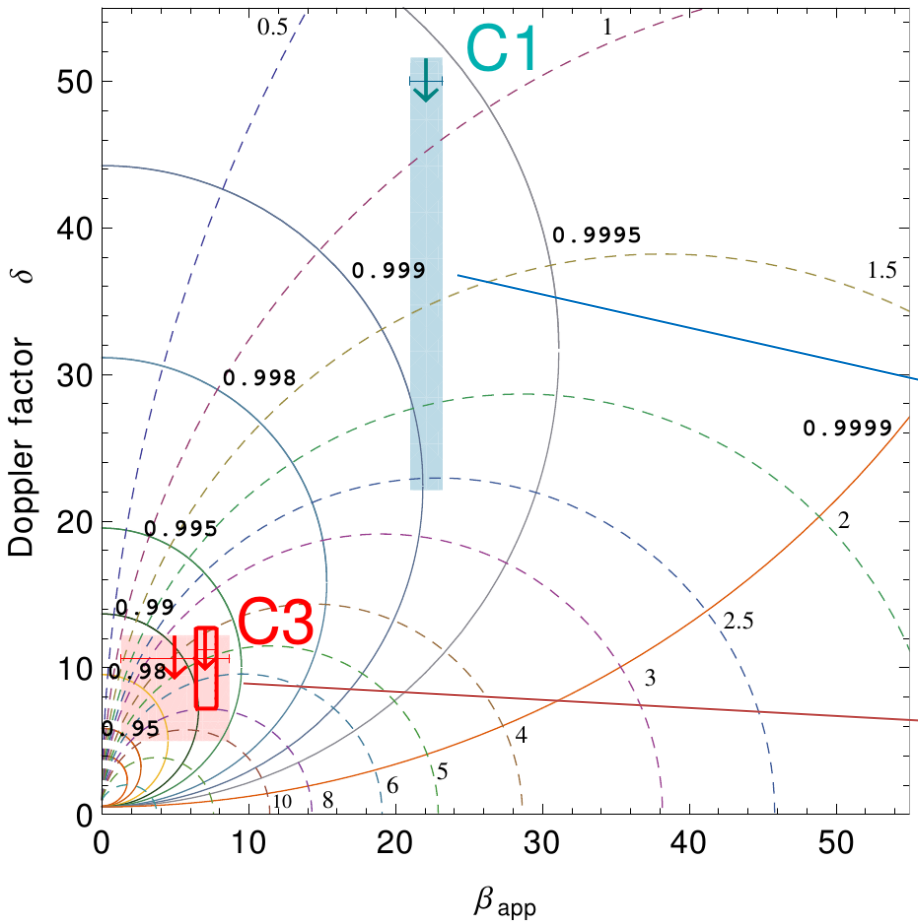

- Components C1 and C3 travel in two distinct regions within the jet
  - C1 at >1 mas and C3 < 0.5 mas

C1: $20 < \gamma < 30$

$0.8^\circ \leq \theta \leq 2.5^\circ$

C3: $7 < \gamma < 10$

$4^\circ \leq \theta \leq 8^\circ$

C1: $22 \leq \delta \leq 50$ and $\beta_{app} \approx 22$

C3: $7 \leq \delta \leq 12$–13 and $\beta_{app} \approx 3$–8

(with conservative error estimates)

Karamanavis et al. 2016a

Intrinsic jet properties

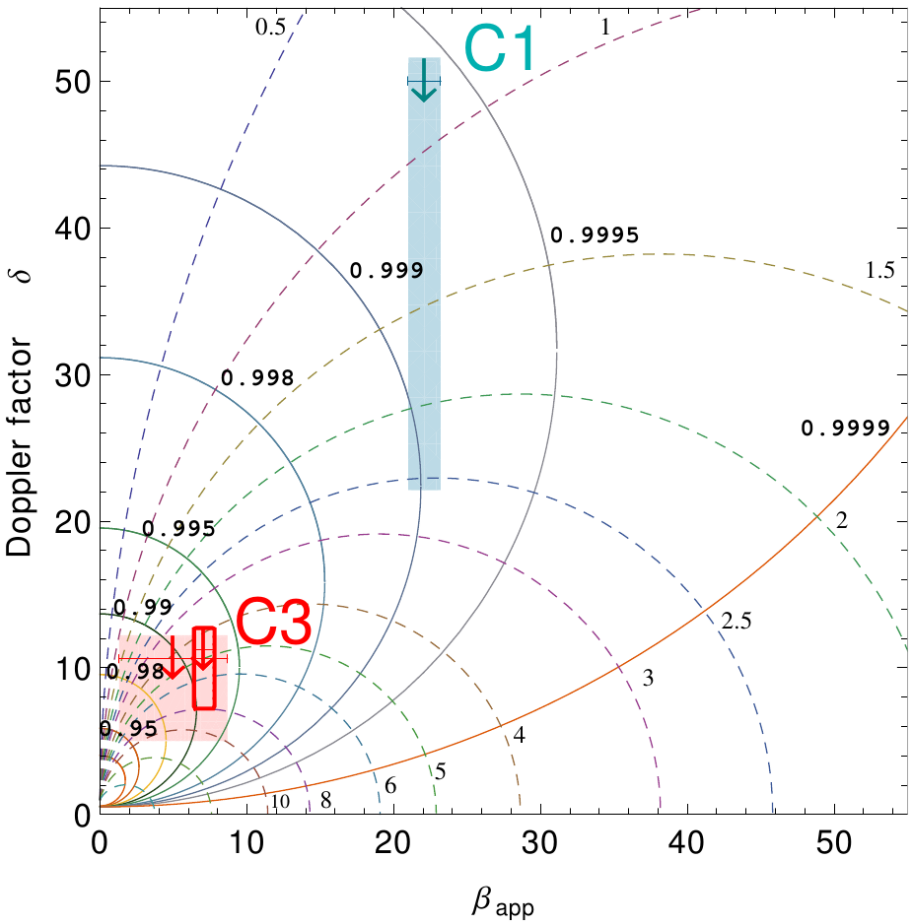

C1: $22 \leq \delta \leq 50$ and $\beta_{app} \approx 22$

C3: $7 \leq \delta \leq 12–13$ and $\beta_{app} \approx 3–8$

(with conservative error estimates)

- The Doppler factor difference (~40) cannot be ascribed only to differential Doppler boosting; i.e. jet bending towards us

- Acceleration must also be taking place within the first mas = 8.5 pc.
  At least, from γ = 10 to 22

Karamanavis et al. 2016a

Flux density evolution of jet features

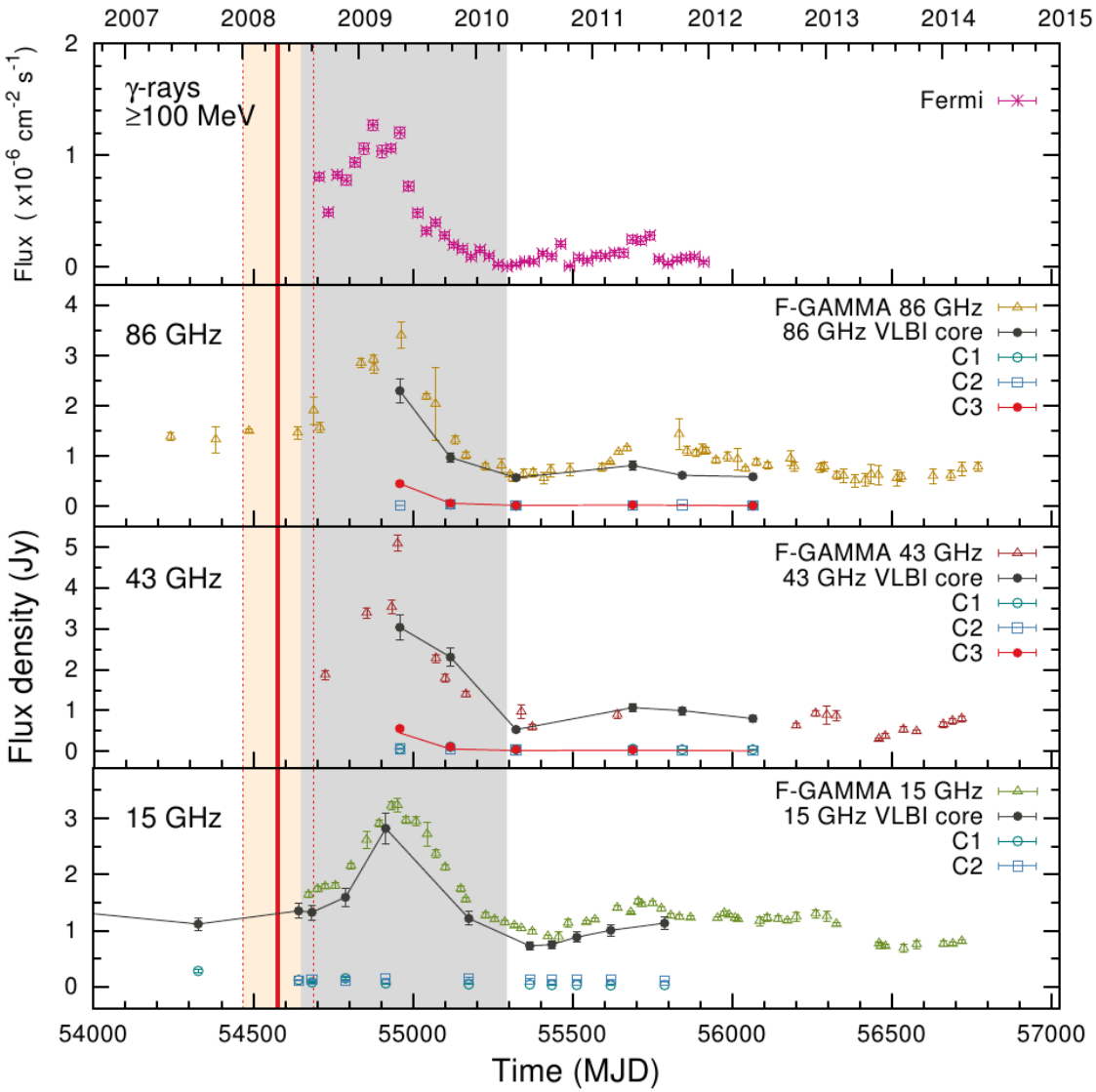

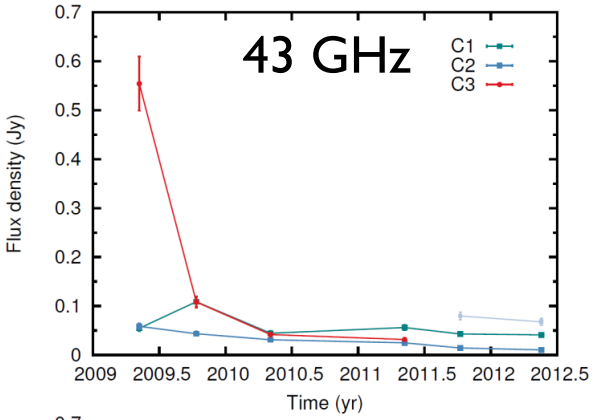

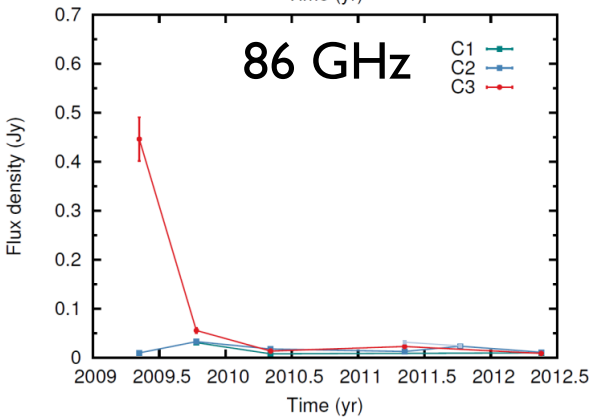

Gray area: Full flare duration

Red line: Ejection time of C3 ± uncertainty

Jet nuclear opacity structure & B-field

ν (GHz)	τ (d)	r_{core} (pc)	$B_{1\,pc}$ $[B_{1\,pc\,min}, B_{1\,pc\,max}]$ (mG)	B_{core} $[B_{core\,min}, B_{core\,max}]$ (mG)
2.64	196.1 ± 11.1	9.91 ± 0.01	169 [93, 314]	17 [9, 32]
4.85	140.9 ± 12.1	7.43 ± 0.02	189 [101, 363]	25 [14, 49]
8.35	106.2 ± 13.8	5.93 ± 0.05	217 [109, 440]	37 [18, 74]
10.45	95.8 ± 15.2	5.52 ± 0.06	235 [114, 495]	43 [21, 90]
14.60	75.2 ± 8.8	4.59 ± 0.08	243 [122, 493]	53 [27, 107]
15.00	61.1 ± 3.1	3.75 ± 0.08	194 [106, 365]	52 [28, 97]
23.05	38.4 ± 4.6	2.62 ± 0.13	174 [91, 340]	66 [35, 130]
32.00	30.8 ± 2.2	2.35 ± 0.17	196 [105, 373]	83 [45, 159]
43.05	36.4 ± 1.4	3.20 ± 0.22	354 [180, 712]	112 [56, 222]
86.24	23.9 ± 0.9	4.12 ± 0.41	807 [370, 1799]	196 [90, 437]
142.33	...	...	...	

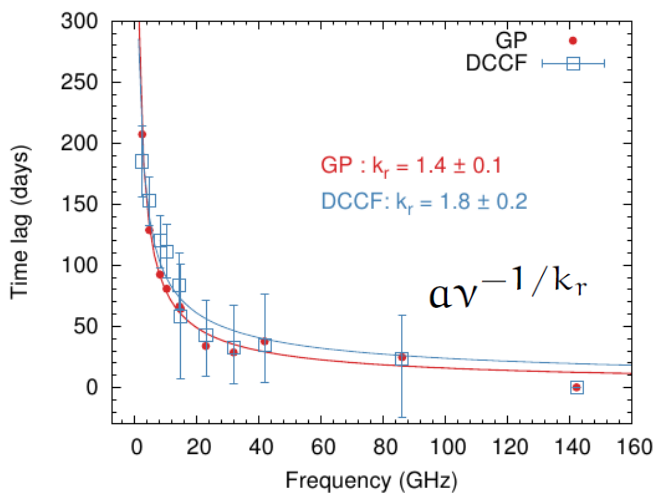

The HE emission site

- From the time-lag core shifts the position of the 86 GHz core can be decisively constrained to ~4.0 pc

- So can the γ-ray emitting region:

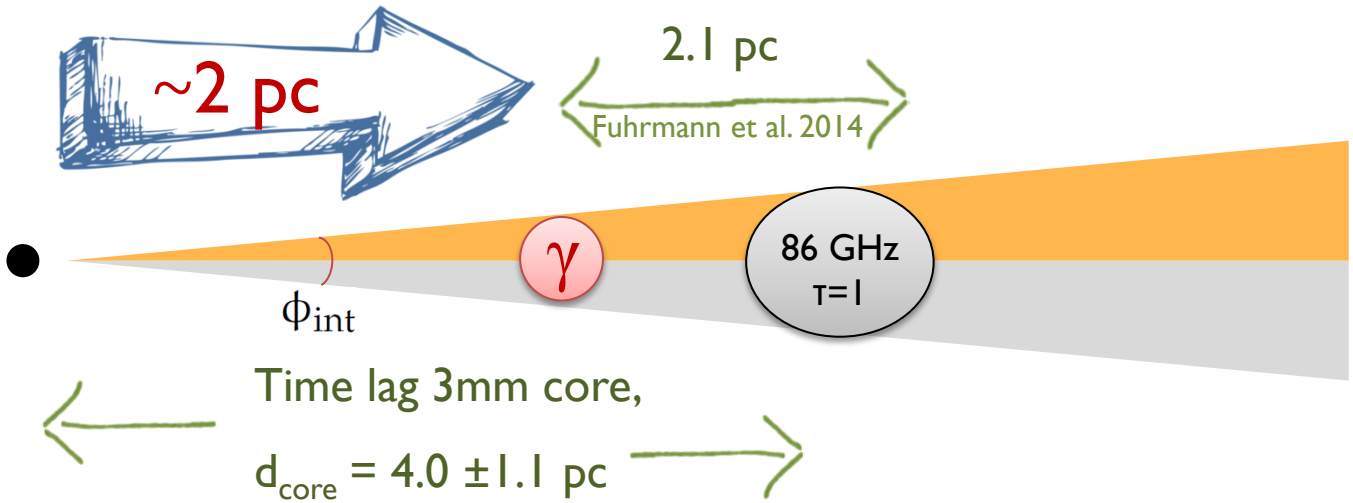

Karamanavis et al. 2016b

The shock origin of component C3

- Different variability mechanisms predict different signatures in the time domain,
- The flare origin can be explored through the comparison of the frequency dependence of light curve parameters:
  - amplitude, time scales, cross-band delays
- …with expectations of the shock-in-jet model (Marscher & Gear 1985)

The shock origin of component C3

Frequency dependence of light curve parameters in agreement with expectations from a shock propagating downstream the jet

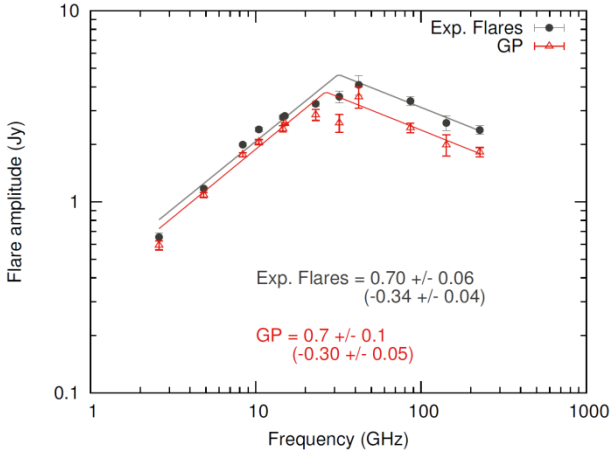

Flare amplitude

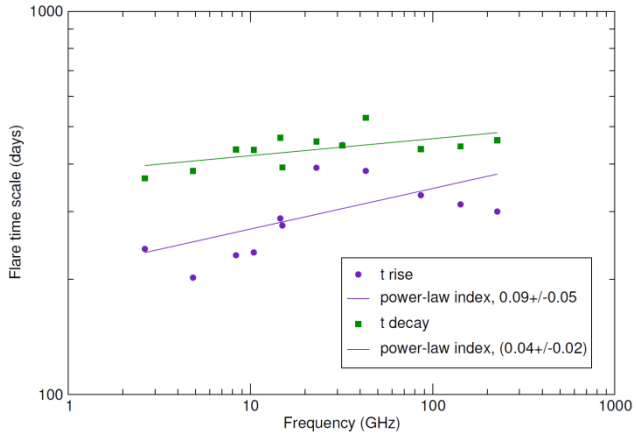

Flare rise & decay time scales

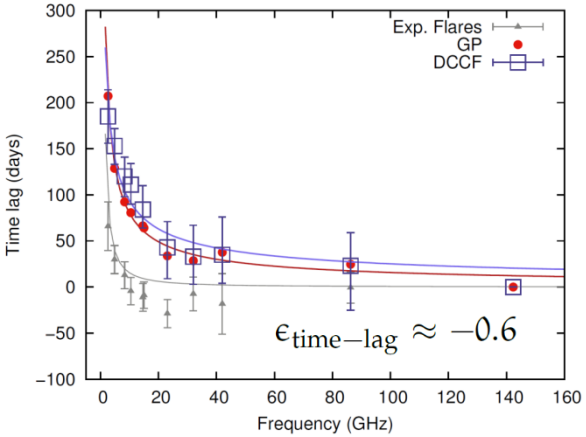

Cross-band delays

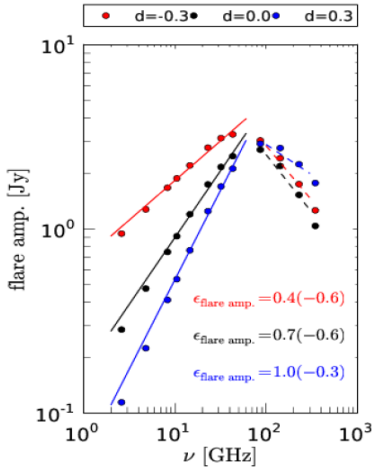

d = -0.3
d = 0
d = 0.3

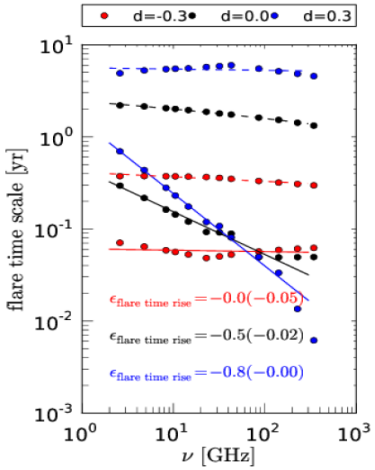

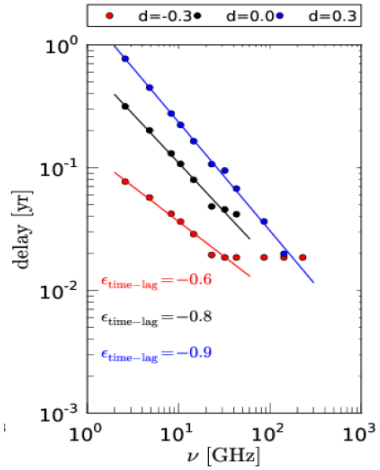

(Fromm et al. 2014)

For the SE kernel, the vector of hyperparameters is $\boldsymbol{\theta} = \{l, \sigma^2\}$ and the probability (or evidence) of the training data y, given the hyperparameters vector $\boldsymbol{\theta}$, is $p(y \mid x, \boldsymbol{\theta})$. The log marginal likelihood is given by

$$\mathcal{L} = \log p(y \mid x, \boldsymbol{\theta}) = -\frac{1}{2} y^T k_n^{-1} y - \frac{1}{2} \log |k_n| - \frac{n}{2} \log 2\pi. \tag{3}$$

More generally, in the case of a hyperparameter vector $\boldsymbol{\theta} = \{\theta_j \mid j = 1, ..., n\}$, the derivatives of the log marginal likelihood with respect to each θ_j are

$$\frac{\partial \mathcal{L}}{\partial \theta_j} = \frac{1}{2} y^T \frac{\partial k_n}{\partial \theta_j} k_n^{-1} y - \frac{1}{2} \operatorname{Trace}\left(k_n^{-1} \frac{\partial k_n}{\partial \theta_j} \right). \tag{4}$$

By means of numerical gradient optimization algorithms one can maximize the log marginal likelihood using Eq. 4 and obtain the best set of hyperparameters (for an outline of the algorithm see [19]).